Spectroscopic factors, overlaps, and isospin symmetry from an *R*-matrix point of view

Carl R. Brune ⦿*

Edwards Accelerator Laboratory, Department of Physics and Astronomy, Ohio University, Athens, Ohio 45701, USA

Background: Spectroscopic factors, overlaps, and isospin symmetry are often used in conjunction with single-particle wave functions for the phenomenological analysis of nuclear structure and reactions. Many differing prescriptions for connecting these quantities to physically relevant asymptotic normalization constants or widths are available in the literature, but their relationship and degree of validity are not always clear.

Purpose: This paper derives relationships among the above quantities of interest using well-defined methodology and starting assumptions.

Method: *R*-matrix theory is used as the primary tool to interoperate among the quantities of interest to this work. Particular attention is paid to effects arising from beyond the nuclear surface, where isospin symmetry is strongly violated.

Results: Relationships between the quantities of interest are derived. Example applications of these methods to mirror levels in nucleon $+ \, ^{12}$C, nucleon $+ \, ^{16}$O, and nucleon $+ \, ^{26}$Al are presented. A new approach to multilevel mirror symmetry is derived and applied to the first three 2^+ states of ^{18}O and ^{18}Ne.

Conclusions: The relationship between the quantities of interest is clarified and certain procedures are recommended. It is found that the asymptotic normalization constant of the second 2^+ state in ^{18}Ne deduced from the mirror state in ^{18}O is significantly larger than found in previous work. This finding has the effect of increasing the ^{17}F$(p, \gamma)^{18}$Ne reaction rate in novae.

I. INTRODUCTION

The concepts of spectroscopic factors, overlaps, and isospin symmetry are widely used for the phenomenological analysis and conceptual understanding of nuclear structure and reactions. These quantities are often used as a "black box," with little understanding of how they relate to each other or to more fundamental descriptions of nuclei. These quantities have physical counterparts, asymptotic normalization constants (ANCs) and widths, that are the relevant ones in experiments and applications. *R*-matrix theory provides a convenient framework for unifying these descriptions.

This work also focuses on energies near nucleon separation thresholds, where significant effects due to the continuum may arise. This energy regime is also a pertinent one for understanding thermonuclear reaction rates in astrophysics, where the use of these concepts has recently been discussed [1,2]. Most of these methods have been developed for many decades, but the results are scattered throughout the literature and in some instances forgotten. There is presently a resurgence of interest in these principles, due to the interest in astrophysical applications and the availability of new radioactive ion beams. In many cases, the determination of astrophysical reaction rates requires the combination of direct measurements, indirect measurements, and theoretical inputs. It is hoped that this paper will be helpful in such efforts.

This paper is organized as follows. First, in Secs. II and III, the concepts of single-particle wave functions and reduced-width amplitudes are introduced. This discussion includes several methods of defining resonances energies and widths as well as computation methods. Most of the calculations in this paper utilize *R*-matrix theory, with the tail of the nuclear potential beyond the channel radii included. This approach allows single-particle quantities, such as widths and ANCs, to be calculated in the typical manner from Woods-Saxon potentials. At the same time, these quantities can be described in the *R*-matrix framework using single-particle reduced-width amplitudes and penetration factors. The inclusion of multiple channels is also straightforward in the *R*-matrix approach. Next, in Sec. IV, the concepts of spectroscopic factors and overlaps are introduced using the same language and connected to *R*-matrix theory. Then, in Sec. V, these concepts are applied to isospin and mirror symmetry. Mirror symmetry is then investigated in Sec. VI using the examples of nucleon $+ \, ^{12}$C, nucleon $+ \, ^{16}$O, and nucleon $+ \, ^{26}$Al. All of these examples involve $\ell = 0$ nucleons and energy levels near the nucleon separation threshold, where the effects of continuum coupling may be significant. Several different approaches are compared. Finally, in Sec. VII, the effect of mirror symmetry operating on a set of levels is considered. In this situation, there is a mixing of the levels due to mirror symmetry breaking beyond the channel radii. The *R*-matrix approach presented here is a new and efficient method for investigating this question. These effects are demonstrated using the first three 2^+ states of ^{18}O and ^{18}Ne. Appendix A describes an

---

*brune@ohio.edu

algorithm that is useful for determining the contribution of the wave-function tail to the overall normalization in a Coulomb potential.

II. SINGLE-PARTICLE WAVE FUNCTIONS

Single-particle wave functions provide a basis for the approximate description of the many-body nuclear physics problem. While the term "single-particle" is appropriate for the nucleon + nucleus case, one can consider these wave functions more generally as one-body wave functions describing a particular two-cluster configuration of a many-body nuclear wave function. The single-particle radial wave function $u(r)/r$ is assumed to satisfy the radial Schrödinger equation

$$-\frac{\hbar^2}{2\mu}\frac{d^2u}{dr^2} + [V(r) + V_C(r)]u + \frac{\hbar^2}{2\mu}\frac{\ell(\ell+1)}{r^2}u = Eu, \quad (1)$$

where $r \geqslant 0$ is the distance between the clusters, E is the relative energy, ℓ is the relative orbital angular momentum quantum number, μ is the reduced mass, and $\hbar$ is Planck's constant. The nuclear single-particle potential $V(r)$ is assumed to be real, central, and local, with $\lim_{r\to 0} r^2V(r) = 0$ and $\lim_{r\to\infty} r^2V(r) = 0$, and $V_C(r)$ is the Coulomb potential. Physical solutions will have $u(r) \propto r^{\ell+1}$ for $r \to 0$, which provides a boundary conditions for $u(0)$. This single-particle wave function is specific to a particular channel, where a channel is defined to be a configuration of given cluster type, total angular momentum, parity, orbital angular momentum, and channel spin. This approach ignores any coupling between different channels.

When the energy E corresponds to a bound or unbound energy level, the single-particle reduced-width amplitude γ is defined by

$$\gamma = u(a)\left(\frac{\hbar^2}{2\mu a \int_0^a u^2\,dr}\right)^{1/2}. \quad (2)$$

The reduced-width amplitude has the physical interpretation of being the amplitude of the resonant wave function at the channel radius, when the wave function is normalized to unity inside the channel radius. All of the ANCs, widths, and reduced widths in this section are derived from single-particle wave functions and are single-particle quantities.

In what follows, I will use r (possibly with a subscript) to indicate an arbitrary radius, b to indicate a large radius where $V(r)$ is negligible, and a to indicate a channel radius, which is located outside the nuclear surface where $V(r)$ is small but not necessarily negligible. In this section, I define the Coulomb functions used in this work and discuss two integral relations that are useful for single-particle states. Then three slightly different ways of defining resonances are introduced and discussed.

A. Coulomb functions

In regions where only the point-Coulomb potential is present, the solutions to Eq. (1) are given by $u = G_\ell(\eta, \rho) \equiv G$ and $u = F_\ell(\eta, \rho) \equiv F$, which are the irregular and regular Coulomb functions, respectively. I also define $\rho = kr$, $k = \sqrt{2\mu E/\hbar^2}$, and $\eta k = Z_1 Z_2 q^2 \mu/\hbar^2$, where $Z_1 q$ and $Z_2 q$ are the charges of the two clusters. The Wronskian relation for the Coulomb functions is

$$G\frac{dF}{dr} - F\frac{dG}{dr} = k. \quad (3)$$

Outgoing and incoming Coulomb waves are defined via

$$O = \exp(-i\sigma)(G + iF) \quad \text{and} \quad (4a)$$

$$I = \exp(i\sigma)(G - iF), \quad (4b)$$

where $\sigma(\ell, \eta)$ is the Coulomb phase shift. One also has

$$O = \exp\left[\frac{\pi}{2}(\eta - i\ell)\right]W_{-i\eta, \ell+1/2}(-2i\rho), \quad (5)$$

where W is the Whittaker function. For E real and negative, such as is the case for bound states, I take $k = i\sqrt{-2\mu E/\hbar^2}$, and W is real. I also consider situations where E is complex, with $\text{Re}\,E > 0$ and $\text{Im}\,E < 0$, in which case the sign of $k = \sqrt{2\mu E/\hbar^2}$ defined such that $\text{Re}\,k > 0$ and k is located near the physical (i.e., real and positive) k axis. The logarithmic derivative of the outgoing solution by

$$L \equiv \frac{r}{O}\frac{dO}{dr}, \quad (6)$$

and when E is real one also defines

$$L \equiv \hat{S} + iP, \quad (7)$$

where $\hat{S}$ and P are the shift and penetration factors, respectively. Note that P vanishes for $E \leqslant 0$. Finally, the phase ϕ is defined by $\tan \phi = F/G$. The functions F, G, O, I, W, L, $\hat{S}$, P, and ϕ are useful for large radii, where $V(r)$ is negligible. They may be continued to smaller radii using the differential equation, Eq. (1), to yield the nuclear-modified Coulomb functions $\mathcal{F}$, $\mathcal{G}$, $\mathcal{O}$, $\mathcal{I}$, $\mathcal{W}$, $\mathcal{L}$, $\hat{S}$, $\mathcal{P}$, and Φ. Where applicable, these modified Coulomb functions obey the same Wronskian relations as the usual Coulomb functions because of the differential equation they satisfy, Eq. (1).

B. Two integral relations

Here I derive two integral relations which enable the extraction of ANCs or widths from the single-particle radial wave function. The first integral relation concerns the energy derivative of the logarithmic radial derivative of u. An early reference for this procedure is given by Lane and Thomas [3, V.1, Eqs. (1.5)–(1.9), p. 283]. Using Eq. (1) with two different solutions u_1 and u_2 corresponding to energies E_1 and E_2, one can show that

$$-\frac{\hbar^2}{2\mu}\frac{d}{dr}\left[u_1\frac{du_2}{dr} - u_2\frac{du_1}{dr}\right] = (E_2 - E_1)u_1 u_2. \quad (8)$$

Upon integrating from $r = r_1$ to r_2, with $r_1 < r_2$, this becomes

$$-\frac{\hbar^2}{2\mu}\left[u_1 u_2\left(\frac{1}{u_2}\frac{du_2}{dr} - \frac{1}{u_2}\frac{du_1}{dr}\right)\right]_{r_1}^{r_2} = (E_2 - E_1)\int_{r_1}^{r_2} u_1 u_2\,dr. \quad (9)$$

Taking $u_1 \to u_2$ yields

$$-\frac{\hbar^2}{2\mu}\left[u^2\frac{\partial}{\partial E}\left(\frac{1}{u}\frac{du}{dr}\right)\right]_{r_1}^{r_2} = \int_{r_1}^{r_2} u^2\,dr, \quad (10)$$

where ∂E is taken at fixed radius. Using the boundary condition on $u(0)$, one can take $r_1 \to 0$ to obtain

$$-\frac{\hbar^2}{2\mu} u^2(r_2) \left[\frac{\partial}{\partial E} \left(\frac{1}{u} \frac{du}{dr} \right) \right]_{r_2} = \int_0^{r_2} u^2 \, dr. \quad (11)$$

The second relation is an application of the two-potential formalism [4, X.V.17, pp. 404–405]. The regular Coulomb wave function F is the solution to Eq. (1) for the point-Coulomb potential alone, $V_{pC} = Z_1 Z_2 q^2 / r$, while u is the solution for $V + V_C$. Taking the differential equation satisfied by u multiplied by F and subtracting the differential equation satisfied by F multiplied by u, I obtain

$$\frac{\hbar^2}{2\mu} \frac{d}{dr} \left(F \frac{du}{dr} - u \frac{dF}{dr} \right) = F(V + V_C - V_{pC}) u. \quad (12)$$

Upon integrating from $r = r_1$ to r_2, with $r_1 < r_2$, this becomes

$$\frac{\hbar^2}{2\mu} \left(F \frac{du}{dr} - u \frac{dF}{dr} \right)_{r_1}^{r_2} = \int_{r_1}^{r_2} F(V + V_C - V_{pC}) u \, dr. \quad (13)$$

I now specify $r_1 \to 0$ and $r_2 = b$, where $V + V_C - V_{pC}$ becomes negligible, and $u(r) = \alpha F(r) + \beta G(r)$ in the vicinity of $r = b$, where α and β are constants. Using the Wronskian relation, Eq. (3), this becomes

$$-\beta \frac{\hbar^2 k}{2\mu} = \int_0^b F(V + V_C - V_{pC}) u \, dr. \quad (14)$$

C. S matrix

The radial wave function may be written as a linear combination of modified Coulomb functions

$$u \propto \mathcal{I} - S\mathcal{O}, \quad (15)$$

where S is the scattering matrix. This relation may also be expressed as

$$u \propto \cos\delta \, \mathcal{F} + \sin\delta \, \mathcal{G}, \quad (16)$$

where δ is the phase shift and

$$S = \exp[2i(\delta + \sigma)]. \quad (17)$$

It is important to note that Eqs. (15) and (16) are valid for any radius, although they will only be used for $r \geqslant a$.

In the S-matrix approach, discrete energy levels may be defined to be those energies where the solution consists of a pure outgoing wave. This provides the usual large-radius boundary condition for bound states, where E is real and negative. For unbound states, this boundary condition can only be achieved for complex E. If there is such an energy level at $E = E_0$, then the S matrix has a first-order pole at the energy such that near $E = E_0$

$$S(E) = \frac{A}{E - E_0} + \text{function that is regular at } E_0, \quad (18)$$

where A is the residue. Using Eq. (15), one finds

$$\frac{1}{u} \frac{du}{dr} = \frac{S^{-1} \frac{d\mathcal{I}}{dr} + \frac{d\mathcal{O}}{dr}}{S^{-1} \mathcal{I} + \mathcal{O}}. \quad (19)$$

The energy derivative of the logarithmic radial derivative of u at $E = E_0$ may then be evaluated by substituting this result

into Eq. (11). By using the Wronskian relation

$$\mathcal{I} \frac{d\mathcal{O}}{dr} - \mathcal{O} \frac{d\mathcal{I}}{dr} = 2ik, \quad (20)$$

one obtains

$$-\frac{2ik}{A} \frac{u^2(r_2)}{\mathcal{O}^2(r_2)} = \frac{2\mu}{\hbar^2} \left[\int_0^{r_2} u^2 \, dr + \frac{\hbar^2}{2\mu r_2} u^2(r_2) \left(\frac{\partial \mathcal{L}}{\partial E} \right)_{r_2} \right]. \quad (21)$$

This equation is independent of r_2, since on the left side one has $u(r) \propto \mathcal{O}(r)$ by definition and Eq. (10) shows the right side is independent of r_2.

If the level is bound, one may normalize the u over all space by requiring that the quantity in brackets on the right side of Eq. (21) is equal to unity. This result can be seen by taking $r_2 \to \infty$ where the surface term vanishes and the usual bound-state normalization condition emerges. It is also shown by Lane and Thomas [3, Eq. (A.29), p. 351]. However, since it is convenient to consider different normalizations, I will leave the normalization unspecified and instead define

$$I_\infty = \int_0^{r_2} u^2 \, dr + \frac{\hbar^2}{2\mu r_2} u^2(r_2) \left(\frac{\partial \mathcal{L}}{\partial E} \right)_{r_2}. \quad (22)$$

One also has

$$\frac{u(r)}{I_\infty^{1/2}} = C \mathcal{W}(r) = C \exp\left[-\frac{\pi}{2} (\eta - i\ell) \right] \mathcal{O}(r), \quad (23)$$

where C is the ANC, which is a real quantity. There is also a simple relationship between the ANC and the residue:

$$C^2 = i \exp[\pi(\eta - i\ell)] \frac{\mu A}{\hbar^2 k}. \quad (24)$$

If the level is unbound, the all-space normalization may also be achieved by normalizing u such that $I_\infty = 1$. In this case, the normalization is less obvious, because the integral is not convergent in the usual sense as $r_2 \to \infty$. However, this regularization procedure has been shown to be useful and also consistent with the Zel'dovich regularization method which involves inserting a convergence factor into the integrand [5–7]. Since the level energy E_0 is complex in this case, one may define the real and imaginary parts according to

$$E_0 = E_S - i \frac{\Gamma_S}{2}, \quad (25)$$

where E_S is the resonance energy defined by the S-matrix pole and Γ_S is the corresponding width. In addition, the pole residue can be used to define a width via

$$\Gamma_{S1} = |A|. \quad (26)$$

In general, $\Gamma_S \neq \Gamma_{S1}$, but they become equal in the limit $\Gamma_S \ll E_S$.

Another expression for Γ_S may be found by multiplying Eq. (1) by u^*, subtracting the complex conjugate, and then integrating [8]:

$$\Gamma_S = i \frac{\hbar^2}{2\mu} \frac{\left(u \frac{du^*}{dr} - u^* \frac{du}{dr} \right)_{r_2}}{\int_0^{r_2} |u|^2 \, dr} \quad (27a)$$

$$= i \frac{\hbar^2}{2\mu r_2} \frac{|u(r_2)|^2 (\mathcal{L}^* - \mathcal{L})_{r_2}}{\int_0^{r_2} |u|^2 \, dr}. \quad (27b)$$

This formula is useful when Γ_S is very small and other approaches to calculating Γ_S may not be accurate [9]. In this situation, one can use the first-order Taylor series

$$\mathcal{L} \approx \hat{\mathcal{S}} + i\mathcal{P} - i\frac{\Gamma_S}{2}\left(\frac{\partial \hat{\mathcal{S}}}{\partial E} + i\frac{\partial \mathcal{P}}{\partial E}\right), \quad (28)$$

where $\hat{\mathcal{S}}$, $\mathcal{P}$, and their energy derivatives are evaluated on the real energy axis at E_S and are real quantities. Defining for convenience an alternative reduced width amplitude

$$|\bar{\gamma}|^2 = \frac{\hbar^2}{2\mu r_2}\frac{|u(r_2)|^2}{\int_0^{r_2}|u|^2\,dr} \quad (29)$$

yields

$$\Gamma_S \approx \frac{2|\bar{\gamma}|^2\mathcal{P}(r_2)}{1 + |\bar{\gamma}|^2\left(\frac{\partial \hat{\mathcal{S}}}{\partial E}\right)_{r_2}}, \quad (30)$$

a formula that is very accurate when $\Gamma_S \ll E_S$. Equations (27) and (30) are valid for all r_2, but are most easily evaluated for $r_2 = b$.

One also has

$$\left[\frac{u(b)}{O(b)}\right]^2 = i\frac{\mu A I_\infty}{\hbar^2 k} \quad (31)$$

for large radii. The integral relation given by Eq. (14) yields

$$\frac{u(b)}{O(b)} = -\frac{2\mu}{\hbar^2 k}\exp(i\sigma)\int_0^b F(V + V_C - V_{pC})\,u\,dr, \quad (32)$$

which provides an alternative method of calculating the residue and hence also the ANC or Γ_{S1}. Finally, by adopting $r_2 = a$ in Eq. (21), the residue may be expressed in terms of the reduced-width amplitude:

$$A = -2i\frac{ka}{O^2(a)}\frac{\gamma^2}{1 + \gamma^2\left(\frac{\partial \mathcal{L}}{\partial E}\right)_a}. \quad (33)$$

D. *R* matrix

In the *R*-matrix approach, the logarithmic derivative of u at the channel radius a is described by the *R* matrix, which is a scalar quantity in the single-channel case. Specifically [3, IV.2, Eq. (2.4), p. 274],

$$\left(\frac{r\,du}{u\,dr}\right)_a = R^{-1} + B, \quad (34)$$

where B is the real boundary condition constant. *R*-matrix energy levels are defined by the poles of the *R* matrix, where the logarithmic derivative of u is B/a. The eigenfunctions satisfying this boundary condition form a complete set inside the channel radius and it can be shown [3, IV, pp. 272–274] that

$$R = \sum_\lambda \frac{\gamma_\lambda^2}{E_\lambda - E}, \quad (35)$$

where γ_λ are the reduced width amplitudes and E_λ are the level energies. Note that these reduced widths, defined as residues of *R*-matrix poles, are completely consistent with the definition given by Eqs. (2), (11), and (34). In order to

investigate a level at an energy E_R in the *R*-matrix approach, it is natural to choose $B = \hat{\mathcal{S}}(E_R)$, the real part of the outgoing wave boundary condition.

If the level is bound, this boundary condition is unchanged from the *S*-matrix case and the results for u are identical. Rewriting Eq. (21) with $r_2 = a$, taking into account the definition of the reduced width amplitude, replacing the residue and $\mathcal{O}$ with the appropriately normalized ANC and $\mathcal{W}$, and noting $\partial \mathcal{L}/\partial E = \partial \hat{\mathcal{S}}/\partial E$ for bound states yield

$$C^2 = \frac{2\mu a}{\hbar^2 \mathcal{W}^2(a)}\frac{\gamma^2}{1 + \gamma^2\left(\frac{\partial \hat{\mathcal{S}}}{\partial E}\right)_a}. \quad (36)$$

If the level is unbound, the boundary condition implies that

$$u(r) = u(a)\frac{\mathcal{F}(a)\mathcal{F}(r) + \mathcal{G}(a)\mathcal{G}(r)}{\mathcal{F}^2(a) + \mathcal{G}^2(a)}. \quad (37)$$

Unlike the other cases, this condition depends somewhat on the value of a. The *R*-matrix expression for the phase shift is

$$\delta = -\Phi(a) + \tan^{-1}\frac{\mathcal{P}(a)}{R^{-1} - \hat{\mathcal{S}}(a) + B}. \quad (38)$$

A convenient definition of the width Γ_R is provided by

$$\left(\frac{d\delta}{dE}\right)_{E_R} = -\left(\frac{d\Phi}{dE}\right)_{E_R} + \frac{2}{\Gamma_R}, \quad (39)$$

that implies

$$\Gamma_R = \frac{2\gamma^2\mathcal{P}(a)}{1 + \gamma^2\left(\frac{\partial \hat{\mathcal{S}}}{\partial E}\right)_a}. \quad (40)$$

Note that this expression for the width is very similar in structure to Eq. (36), the equation for the ANC. For unbound states, the integral relation given by Eq. (14) yields

$$\frac{u(a)\mathcal{G}(a)}{\mathcal{F}^2(a) + \mathcal{G}^2(a)} = -\frac{2\mu}{\hbar^2 k}\int_0^b F(V + V_C - V_{pC})\,u\,dr, \quad (41)$$

which provides another way to calculate the reduced-width amplitude. Note that unbound states in the *R*-matrix approach cannot be normalized to unity over all space via the regularization procedure that may be applied for the case of Gamow states. The normalization is left unspecified, although it is often assumed that $\int_0^a u^2\,dr = 1$.

E. *K* matrix

Here I will consider an unbound state with a *K*-matrix boundary condition, where the resonance energy is defined to have a phase shift of $\delta = \pi/2 + m\pi$, where m is an integer and $u(r) \propto \mathcal{G}(r)$ at the resonance energy (see the work of Humblet [10, Eq. 9.4]). Using

$$\frac{1}{u}\frac{du}{dr} = \frac{\cos\delta\,\frac{d\mathcal{F}}{dr} + \sin\delta\,\frac{d\mathcal{G}}{dr}}{\cos\delta\,\mathcal{F} + \sin\delta\,\mathcal{G}}, \quad (42)$$

one finds at a *K*-matrix resonance

$$\left[\frac{\partial}{\partial E}\left(\frac{r\,du}{u\,dr}\right)\right]_{r_2} = \left[\frac{\partial}{\partial E}\left(\frac{r\,d\mathcal{G}}{\mathcal{G}\,dr}\right)\right]_{r_2} - \frac{kr_2}{\mathcal{G}^2(r_2)}\frac{d\delta}{dE}. \quad (43)$$

TABLE I. Effect of the resonance definition on the resonance energy (E_S, E_R, and E_K) and resonance width (Γ_S, Γ_{s1}, Γ_R, and Γ_K), for three situations.

System	$n\ell$	E_S (keV)	E_R (keV)	E_K (keV)	$\dfrac{E_S - E_R}{\Gamma_S}$	$\dfrac{E_S - E_K}{\Gamma_S}$	Γ_S (keV)	Γ_{S1} (keV)	Γ_R (keV)	Γ_K (keV)
$p + {}^{12}$C	$2s$	420.5	424.0	424.1	-0.0921	-0.0935	37.50	35.85	39.17	39.23
$p + {}^{14}$N	$2s$	259.3	259.3	259.3	-0.0072	-0.0072	1.173	1.169	1.173	1.173
$p + {}^{26}$Al	$2s$	126.8	126.8	126.8			4.96×10^{-9}	4.96×10^{-9}	4.96×10^{-9}	4.96×10^{-9}

The K-matrix width Γ_K may be defined at the K-matrix resonance energy E_K via

$$\left(\frac{d\delta}{dE} \right)_{E_K} = \frac{2}{\Gamma_K}. \qquad (44)$$

Then, using Eqs. (11) and (43), one finds

$$\Gamma_K = \frac{\hbar^2 k}{\mu} \frac{u^2(r_2)}{\mathcal{G}^2(r_2)} \left\{ \int_0^{r_2} u^2 \, dr \right.$$
$$\left. + \frac{\hbar^2}{2\mu r_2} u^2(r_2) \left[\frac{\partial}{\partial E} \left(\frac{r}{\mathcal{G}} \frac{d\mathcal{G}}{dr} \right) \right]_{r_2} \right\}^{-1}. \qquad (45)$$

The integral relation given by Eq. (14) yields

$$\frac{u(b)}{G(b)} = -\frac{2\mu}{\hbar^2 k} \int_0^b F(V + V_C - V_{pC}) \, u \, dr. \qquad (46)$$

F. Practical calculations

For calculations, I assume that $V(r)$ is described by a phenomenological Woods-Saxon potential

$$V(r) = \frac{-V_0}{1 + \exp[(r - R_n)/a_n]} \qquad (47)$$

and the Coulomb potential is given by a uniformly charged sphere of radius R_C. In this work, numerical calculations will only be performed for nucleon + A-nucleon configurations, although all equations are completely general and apply, for example, to α + nucleus channels. It is assumed that $R_n = r_n A^{1/3}$ and $R_C = r_C A^{1/3}$, with $r_n = r_C = 1.25$ fm and a diffuseness parameter of $a_n = 0.65$ fm, unless otherwise specified. The potential depth V_0 is often adjusted to reproduce the level energy and n, the number of radial nodes inside the channel radius (including the origin). When E is complex, $u(r)$ is likewise complex, and the nodes are counted using the real part of $u(r)$, where the phase of $u(r)$ is fixed such that $u(r)$ is real and positive near $r = 0$.

Equation (1) is solved numerically via the Numerov method. In the case of u, either the potential depth is varied to generate the desired level energy or the level energy is determined for a fixed potential. One solution is propagated outward from $r = 0$, starting with $u(0) = 0$. Another solution is propagated inward from $r = b$, starting with the desired boundary condition. The solutions are compared at the channel radius $r = a$. The level energy or potential depth is then varied to reproduce the desired n value and match the logarithmic derivatives at the channel radius. The modified Coulomb functions are also found by numerical integration,

starting with the unmodified Coulomb functions at $r = b$ and integrating inward to $r = a$. I utilize $a = R_n + a_n$, unless otherwise specified, and $b = 20$ fm.

In the preceding development, energy derivatives of $\mathcal{L}$, $\hat{S}$, $\mathcal{P}$, and $(r/\mathcal{G})(d\mathcal{G}/dr)$ play an important role. For $r = b$, where the Coulomb functions are unmodified, $\partial L/\partial E$ can be efficiently calculated using the continued fraction algorithm given in Appendix A. This algorithm is of general use for the normalization of bound and Gamow states, as well as for R-matrix calculations. For smaller radii, one has from Eq. (10)

$$-\frac{\hbar^2}{2\mu} \left[\frac{\mathcal{O}^2}{r} \left(\frac{\partial \mathcal{L}}{\partial E} \right) \right]_{r_1}^{b} = \int_{r_1}^{b} \mathcal{O}^2 \, dr \qquad (48)$$

that allows $\partial \mathcal{L}/\partial E$ at smaller radii to be calculated from $\partial L/\partial E$ at $r = b$ and an integration. Since $\mathcal{L} = \hat{S} + i\mathcal{P}$, this method takes care of three out of four of the needed energy derivatives. Alternatively, $\partial \mathcal{L}/\partial E$ may be calculated by numerical differentiation, an approach that also works for the remaining case, the energy derivative of $(r/\mathcal{G})(d\mathcal{G}/dr)$, that in practice is only needed for $r = b$.

G. Discussion

The different resonance definitions do give rise to somewhat different resonance energies and widths when the resonances become broad. This effect has been investigated by considering $\ell = 0$ resonances in $p + {}^{12}$C, $p + {}^{14}$N, and $p + {}^{26}$Al. The potential depth was adjusted once to reproduce the resonance energy for R-matrix definition, and was then left constant for the calculation with the other definitions. The results are shown in Table I, where the resonance energy for $p + {}^{12}$C is from Ref. [11], that for $p + {}^{14}$N is from Ref. [12], and that for $p + {}^{26}$Al is from Refs. [13,14]. Because of the variable Coulomb barrier and resonance energy, the single-particle width vary considerably. In the case of $p + {}^{12}$C, the single-particle width is just under 10% of the resonance energy and non-negligible differences in the resonance energies and widths are seen. The differences in resonance energy are seen to be a small fraction of the resonance width.

These differences are easily understood. For example, the single-channel S and R matrices are related via

$$S = \frac{2i\rho}{\mathcal{O}^2} (R^{-1} - \hat{S} - i\mathcal{P} + B)^{-1} + \frac{\mathcal{I}}{\mathcal{O}}. \qquad (49)$$

The energy dependence of the shift and penetration factors may be approximated using

$$\hat{S} + i\mathcal{P} \approx B + i\mathcal{P}_R + (E - E_R) \left(\frac{\partial \hat{S}}{\partial E} + i \frac{\partial \mathcal{P}}{\partial E} \right)_{E_R}, \qquad (50)$$
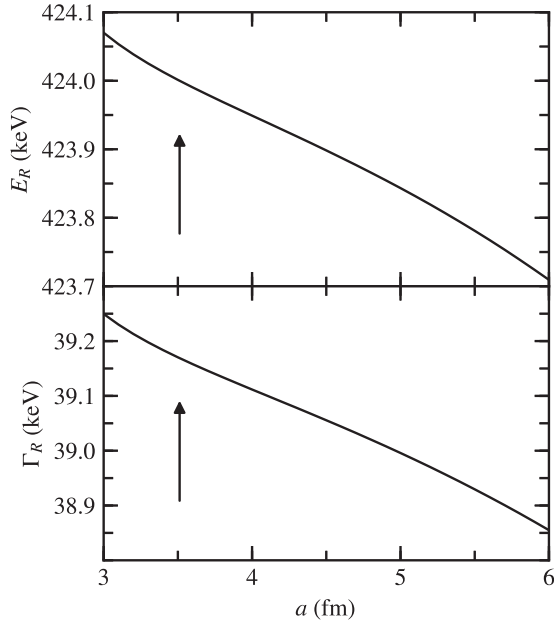
FIG. 1. The dependence of the R-matrix $p + {}^{12}\text{C}$ resonance energy and width on the channel radius. The arrows indicate the channel radius of 3.51 fm used for the calculations reported in Table I.

where $\mathcal{P}_R$ and the energy derivatives are evaluated at E_R. Making a single-level approximation to R then allows the S- and R-matrix pole positions to be related:

$$E_S - i\frac{\Gamma_S}{2} \approx E_R - i\frac{\gamma^2 \mathcal{P}_R}{1 + \gamma^2 \left(\frac{\partial \hat{\mathcal{S}}}{\partial E} + i\frac{\partial \mathcal{P}}{\partial E}\right)_{E_R}}, \qquad (51)$$

where γ is the R-matrix reduced width.

The R-matrix resonance energy and width also have some dependence on the value of the channel radius. This variation is shown for the case of the $p + {}^{12}\text{C}$ resonance and $3 \leqslant a \leqslant 6$ fm in Fig. 1, where both E_R and Γ_R are seen to vary by about 0.4 keV. However, the E_S and Γ_S calculated from the R-matrix pole parameters using Eq. (51) only vary within 0.12 and 0.05 keV, respectively.

The differences between the various resonance energy and width definitions are small, unless the width is not small compared to the resonance energy. Different resonance energy definitions are also discussed in Ref. [15], where similar conclusions are reached. These approaches should be viewed as different, but equivalent, descriptions of the same resonance. In practice, if the choice matters, it should be dictated by consistency with how the single-particle state is used. If a transfer reaction or R-matrix calculation is coupled to a single-particle calculation, consistent resonance definitions should be utilized throughout. For example, some versions of the transfer reaction code DWUCK4 [16] utilizes the K-matrix boundary condition to define a resonant state. In addition, if the resonance is not narrow, it is unlikely to be a good approximation to treat it in isolation. Rather, the effects of potential scattering and/or interference with other resonances will be significant.

Although the S- and K-matrix approaches are formally independent of the channel radius, all three approaches can

also be unified from a generalized R-matrix point of view with a channel radius [17]. See also [18] for the S-matrix pole expansion using a channel radius. In the K-matrix case, the results can be recast into R-matrix form by noting the K-matrix boundary condition corresponds to adopting $B = (r/\mathcal{G})(d\mathcal{G}/dr)$ at the channel radius. For the remainder of this work, I will utilize the R-matrix definition of resonances parameters almost exclusively.

It should also be kept in mind that these results depend to various degrees on the single-particle potential parameters and channel radius. The reduced widths vary with radius of the nuclear potential (which depends on A), the orbital angular momentum, and number of radial nodes. The systematics of these variations have been studied by Iliadis [19], where substantial variations are seen, even if the reduced width is made dimensionless. The variation of the single-particle reduced width with charge and energy is weaker, provided the energy variation stays within a few MeV of the separation threshold. The reason for this observation is that Coulomb energy difference or potential energy change is relatively small compared to the depth of the nuclear potential, which accordingly leads to a small change in the wave function inside the channel radius.

III. FURTHER DEVELOPMENT

A. Effect of the nuclear potential on the penetrability

By including the attractive tail of the nuclear potential in the calculation of the Coulomb functions, the penetration factors are increased compared to a Coulomb-only calculation. The advantage of this approach is that single-particle ANCs and widths calculated from potentials with a tail, such as the Woods-Saxon potential used here, can be expressed using R-matrix formulas involving single-particle reduced-width amplitudes, such as shown by Eqs. (36) and (40). Here, I consider the *penetrability ratio* defined to be the ratio of the penetration factor calculated with the nuclear potential included to that calculated without. This ratio can be defined for any energy to be $|O(a)/\mathcal{O}(a)|^2$. When the energy is real and positive, this becomes $\mathcal{P}(a)/P(a)$ since $\mathcal{P}(a) = ka/[\mathcal{F}^2(a) + \mathcal{G}^2(a)]$ and $P(a) = ka/[F^2(a) + G^2(a)]$ in this case. For bound states, with E real, the ratio is given by $W^2(a)/\mathcal{W}^2(a)$. This ratio is shown in Figs. 2 and 3 for the cases of nucleon $+ {}^{12}\text{C}$ and nucleon $+ {}^{26}\text{Al}$, for three $n\ell$ values and real energies. For these calculations, the nuclear well depth has been adjusted to place the single-particle level energy at the energy of the ratio calculation, using the R-matrix boundary condition. The ratios are seen to be moderately increased from unity, reasonably independent of energy, and continuous across $E = 0$. The results for $n + {}^{12}\text{C}$ are similar to those reported by Johnson [20, Fig. 4] for $n + {}^{16}\text{O}$ with a fixed well depth.

B. Volume renormalization factor

In the single-channel case, the volume renormalization factor for R-matrix states is given by

$$\left[1 + \gamma^2 \left(\frac{\partial \hat{\mathcal{S}}}{\partial E}\right)_a\right]^{-1}, \qquad (52)$$
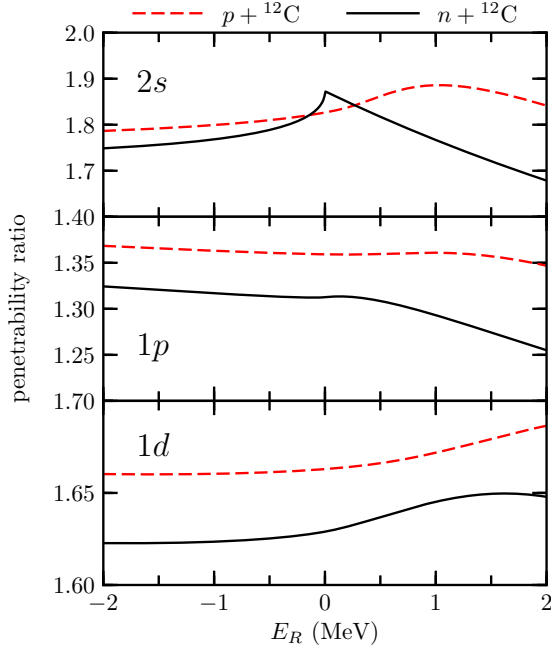
FIG. 2. The penetrability ratio as a function of the level energy for $p + {}^{12}\text{C}$ and $n + {}^{12}\text{C}$ for $n\ell = 2s$, $1p$, and $1d$. See Sec. III A for details.

which appears in many places in this work, including the definitions of single-particle ANCs, Eq. (36) and single-particle widths, Eq. (40). In the many-channel case, this quantity
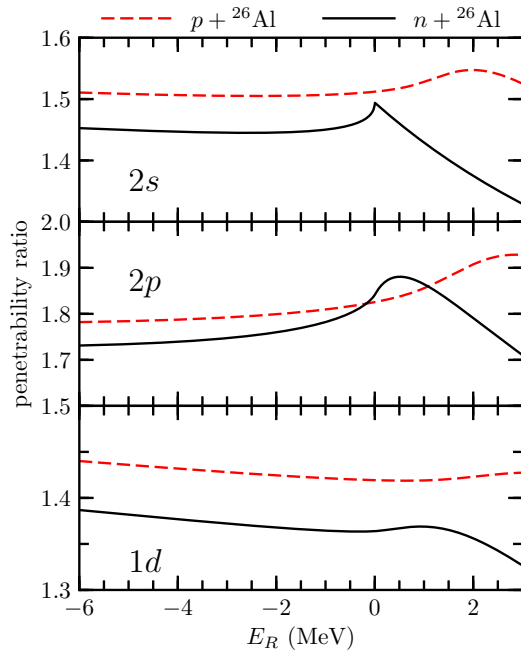

FIG. 3. The penetrability ratio as a function of the level energy for $p + {}^{26}\text{Al}$ and $n + {}^{26}\text{Al}$ for $n\ell = 2s$, $2p$, and $1d$. See Sec. III A for details.
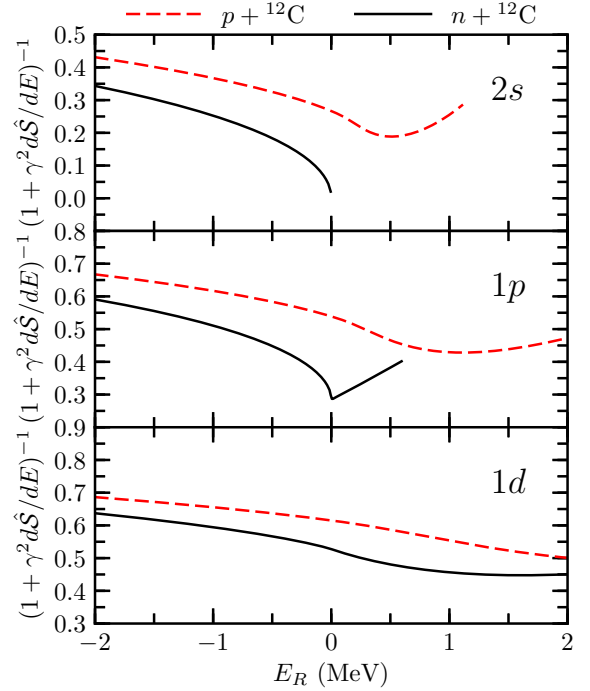

FIG. 4. The volume renormalization for $p + {}^{12}\text{C}$ and $n + {}^{12}\text{C}$, for the single-channel case and the single-particle reduced width.

generalizes to

$$\left[1 + \sum_c \gamma_c^2 \left(\frac{\partial \hat{\mathcal{S}}_c}{\partial E} \right)_{a_c} \right]^{-1}. \tag{53}$$

It likewise appears in several contexts below, including Eqs. (68), (70), and (80). The volume renormalization factor for Gamow states, where $\hat{\mathcal{S}}$ is replaced by $\mathcal{L}$, is very similar, being identical in the case of bound states and having a small complex component for narrow resonances. Examples of the volume renormalization factor for nucleon $+ {}^{12}\text{C}$ and nucleon $+ {}^{26}\text{Al}$ are shown in Figs. 4 and 5, for low partial waves. These calculations are for the single-channel case and assuming the single-particle reduced width. The factor differs significantly from unity in all cases, with the largest differences being near the nucleon separation threshold. For $\ell = 1$ neutrons, a cusp at the threshold is produced.

It should be noted that this factor appears in several other contexts besides the ones discussed in this paper. For example, it can be used to explain threshold anomaly [21,22] observed in (d, p) reactions on heavy nuclei. It also arises in the explanation of why states with a significant single-particle structure tend to be located near separation thresholds [23]. In both of these cases, the factor is describing the excitation energy compression for physical resonant states that is caused by a channel threshold. A more detailed mathematical model for this compression is provided by the transformation methods described in Appendix B of this work. In this picture, the compression occurs when one transforms from eigenstates satisfying constant logarithmic boundary conditions to resonant boundary conditions.
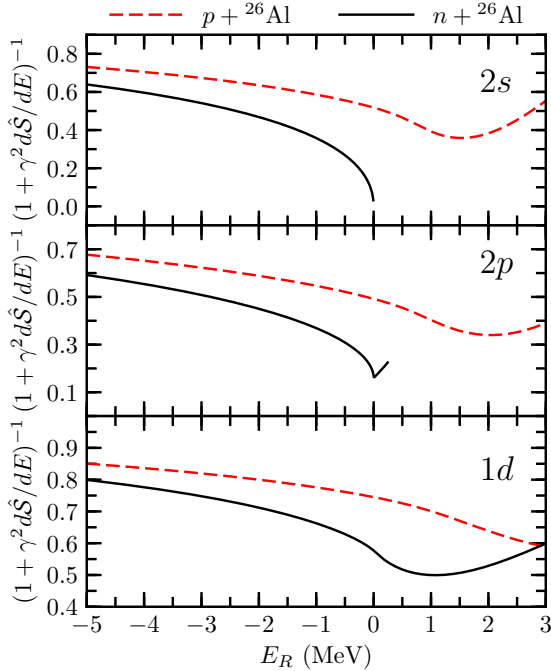
FIG. 5. The volume renormalization for $p + {}^{26}\mathrm{Al}$ and $n + {}^{26}\mathrm{Al}$, for the single-channel case and the single-particle reduced width.

IV. OVERLAPS, SPECTROSCOPIC FACTORS, AND REDUCED WIDTH AMPLITUDES

The radial overlap function $\mathcal{R}_c(r)$ is the projection of a many-body nuclear wave function on to a particular channel configuration [24–32] that satisfies an inhomogeneous Schrödinger-like equation. For large r, $\mathcal{R}_c(r)$ satisfies a one-body radial Schrödinger equation with the intercluster Coulomb potential and the cluster separation energy. Here, channels denote a two-cluster configuration with quantum numbers discussed in the first paragraph of Sec. II. Channels will be labeled with the subscript c when necessary. The overlap function allows one to link together the spectroscopic factor, reduced-width amplitude, and many-body theoretical calculations.

A. Computational point of view

If the many-body wave function $|\Psi\rangle$ is known, for example, by finding the eigensolution to a given Hamiltonian, then the overlap function may be calculated. One may then define spectroscopic factors according to [33]

$$\mathcal{S}_c = \int_0^\infty \mathcal{R}_c^2(r)\, r^2\, dr, \tag{54}$$

where it assumed that the wave function is normalized to unity over all space, i.e., $\langle \tilde{\Psi} | \Psi \rangle_0^\infty \equiv 1$. Because of the normalization convention, the spectroscopic factor can only be strictly defined for Gamow states. In this work, I refer to multichannel states as Gamow states if they have outgoing waves in all channels. This definition includes bound states. It is also useful to define the spectroscopic amplitude whose

square is the spectroscopic factor

$$\mathcal{S}_c = \mathcal{A}_c^2. \tag{55}$$

Note that the spectroscopic factor and amplitude, as defined here, include an isospin Clebsch-Gordan factor that is discussed below in Sec. V. Time-reversal invariance allows $\mathcal{R}_c$, $\mathcal{S}_c$, and $\mathcal{A}_c$ to be defined as real quantities when the energy of the state is real.

The reduced-width amplitude is defined according to [3, III.4, Eq. (4.8a), p. 271]

$$\gamma_c = \left(\frac{\hbar^2 a_c}{2\mu_c \langle \tilde{\Psi} | \Psi \rangle_0^a} \right)^{1/2} \mathcal{R}_c(a_c), \tag{56}$$

where the factor $\langle \tilde{\Psi} | \Psi \rangle_0^a$ implements the R-matrix convention that the wave function is normalized to unity *inside* the channel radii. When the energy is real, $\langle \tilde{\Psi} | \Psi \rangle_0^a$ is real, positive, and less than 1. Because the normalization is not extended to infinity, reduced widths may be defined for a much broader class of states, including unbound R-matrix eigenstates. The single-channel R-matrix resonance condition given in Sec. II D generalizes naturally to

$$\left[\frac{1}{\mathcal{R}_c} \frac{d(r\mathcal{R}_c)}{dr} \right]_{a_c} = [\hat{\mathcal{S}}_c]_{a_c}, \tag{57}$$

for all channels and at the level energy. This represents the real part of the outgoing wave boundary condition.

It should be noted that spectroscopic factors are subject to some theoretical ambiguity arising from from how the underlying nuclear interactions are defined [29,34,35]. On the other hand, widths and ANCs, which are asymptotic quantities, are free from such ambiguities. The reduced width amplitude, being nearly asymptotic, is also essentially free from this issue.

B. Phenomenological point of view

In the phenomenological approach, neither the Hamiltonian nor the wave function are assumed to be known. One instead works directly with level energies, ANCs, and partial widths. In addition, the radial overlap function may be approximated using the replacement

$$\mathcal{R}_c(r) \rightarrow \mathcal{A}_c \frac{u_c(r)}{r}, \tag{58}$$

where $u_c(r)/r$ is the single-particle radial wave function, as discussed in Sec. II. Provided that $u_c(r)$ is normalized such that $I_\infty = 1$ via Eq. (22), this replacement is consistent with Eq. (54). This approximation is commonly used in transfer reaction calculations. In bound channels, one then finds for the square of the ANC

$$C_c^2 = \mathcal{S}_c C_{c,\mathrm{sp}}^2, \tag{59}$$

where $C_{c,\mathrm{sp}}^2$ is the square of the single-particle ANC given by Eqs. (23), (24), or (36). For unbound channels, the partial width is given by

$$\Gamma_c = \mathcal{S}_c \Gamma_{c,\mathrm{sp}}, \tag{60}$$

where $\Gamma_{c,\mathrm{sp}}$ is the single-particle partial width. Strictly speaking, the single-particle partial width should be taken as Γ_{S1},

as defined Eq. (26), since $\mathcal{A}_c$ scales the asymptotic single-particle wave function. However, as discussed in Sec. II G, all of the width definitions are approximately equivalent if the single-particle width is narrow.

In a phenomenological analysis, the number of channels is limited to one or a small number. Those with a large spectroscopic factor, small separation energy, and/or low orbital angular momentum are likely to be important and should be included. As discussed in Sec. II A, it is assumed that the Coulomb functions can be extended inward to the channel radii, including the effects of the nuclear single-particle potential. This approach has been utilized in several studies, including Refs. [20,36–39]. While this procedure is a very reasonable approximation where the tail of the nuclear potential is concerned, it does have some limitations. Since the true overlap functions satisfy an inhomogeneous radial equation (see, e.g., Ref. [30]), there will be small violations of the Wronskian relation satisfied by the modified Coulomb functions. Also, Robson [37, pp. 494–495] has noted that using channel radii just outside the nuclear surface gives rise to some mild nonorthogonality between the channels. These effects could be removed by using larger channel radii, but that would introduce additional breaking of isospin symmetry. I agree with Robson [37] that channel radii just outside the nuclear surface are the best choice for phenomenological analyses when isospin symmetry is utilized.

In the phenomenological approach, the extension of $\mathcal{R}_c(r)$ for a Gamow state beyond the channel radii is given by

$$\mathcal{R}_c(r) = \mathcal{R}_c(a_c) \frac{\mathcal{O}_c(r)/r}{\mathcal{O}_c(a_c)/a_c} \tag{61a}$$

$$= \gamma_c \left(\frac{2\mu_c \langle \tilde{\Psi} | \Psi \rangle_0^a}{\hbar^2 a_c} \right)^{1/2} \frac{\mathcal{O}_c(r)/r}{\mathcal{O}_c(a_c)/a_c}, \tag{61b}$$

where Eq. (56) has been utilized. Equation (10) implies

$$\int_{a_c}^{\infty} \frac{\mathcal{O}_c(r)}{\mathcal{O}_c(a_c)} \, dr = \frac{\hbar^2}{2\mu_c a_c} \left(\frac{\partial \mathcal{L}_c}{\partial E} \right)_{a_c}, \tag{62}$$

which is a regularized value if the channel is unbound. One then has

$$\int_{a_c}^{\infty} \mathcal{R}_c^2(r) \, r^2 \, dr = \gamma_c^2 \langle \tilde{\Psi} | \Psi \rangle_0^a \left(\frac{\partial \mathcal{L}_c}{\partial E} \right)_{a_c}. \tag{63}$$

The normalization condition $\langle \tilde{\Psi} | \Psi \rangle_0^\infty \equiv 1$ may be expressed as

$$\langle \tilde{\Psi} | \Psi \rangle_0^a + \sum_c \int_{a_c}^{\infty} \mathcal{R}_c^2(r) \, r^2 \, dr = 1, \tag{64}$$

which yields

$$\langle \tilde{\Psi} | \Psi \rangle_0^a = \left[1 + \sum_c \gamma_c^2 \left(\frac{\partial \mathcal{L}_c}{\partial E} \right)_{a_c} \right]^{-1}. \tag{65}$$

This is a generalization of the well-known volume renormalization factor in R-matrix theory [3, IV.7, p. 280; Eqs. (A.29) and (A.30), p. 351] that is discussed above in Sec. III B.

Equations (2) and (22), with $I_\infty = 1$, yield

$$\frac{\hbar^2}{2\mu_c a_c} \frac{u_c^2(a_c)}{\gamma_{c,\mathrm{sp}}^2} = \left[1 + \gamma_{c,\mathrm{sp}}^2 \left(\frac{\partial \mathcal{L}_c}{\partial E} \right)_{a_c} \right]^{-1}. \tag{66}$$

The square of Eq. (56), with the replacement $\mathcal{R}_c^2(a_c) \to \mathcal{S}_c u_c^2(a_c)/a_c^2$, then provides

$$\frac{\gamma_c^2}{1 + \sum_{c'} \gamma_{c'}^2 \left(\frac{\partial \mathcal{L}_{c'}}{\partial E} \right)_{a_{c'}}} = \mathcal{S}_c \frac{\gamma_{c,\mathrm{sp}}^2}{1 + \gamma_{c,\mathrm{sp}}^2 \left(\frac{\partial \mathcal{L}_c}{\partial E} \right)_{a_c}}. \tag{67}$$

With these equations, it is straightforward to interoperate fully among the single-particle wave functions and spectroscopic factors and among the single-particle and actual ANCs, partial widths, and reduced widths. For a state bound in channel c, Eqs. (36), (59), and (67) may be combined to yield

$$C_c^2 = \frac{2\mu_c a_c}{\hbar^2 \mathcal{W}_c^2(a_c)} \frac{\gamma_c^2}{1 + \sum_{c'} \gamma_{c'}^2 \left(\frac{\partial \hat{\mathcal{S}}_{c'}}{\partial E} \right)_{a_{c'}}}, \tag{68}$$

which is the general relation between the ANC and the reduced widths. For a state that is unbound in channel c, one may likewise combine Eqs. (26), (33), and (67) to obtain

$$\Gamma_c = 2 \left| \frac{k_c a_c}{\mathcal{O}_c^2(a_c)} \frac{\gamma_c^2}{1 + \sum_{c'} \gamma_{c'}^2 \left(\frac{\partial \mathcal{L}_{c'}}{\partial E} \right)_{a_{c'}}} \right|, \tag{69}$$

where this is the partial width defined by the S-matrix pole residue. The corresponding partial width for the R-matrix definition is

$$\Gamma_c = 2\mathcal{P}_c(a_c) \frac{\gamma_c^2}{1 + \sum_{c'} \gamma_{c'}^2 \left(\frac{\partial \hat{\mathcal{S}}_{c'}}{\partial E} \right)_{a_{c'}}}, \tag{70}$$

with all of the terms in this formula being real quantities. In what follows, it is useful to unify the treatment of bound and unbound channels by defining

$$X_c = \begin{cases} \frac{\hbar^2 \mathcal{W}_c^2(a_c) C_c^2}{2\mu_c a_c} & \text{bound channel} \\[2ex] \frac{\Gamma_c}{2\mathcal{P}_c(a_c)} & \text{unbound channel} \end{cases}, \tag{71}$$

where the R-matrix definition of the partial width is utilized.

It should be noted that low-energy nuclear physics experiments are insensitive to short-range features of nuclear wave functions. Consequently, neither the single-particle potential nor the spectroscopic factor are well constrained from a phenomenological point of view. However, ANCs, widths, and reduced widths, being asymptotic or nearly asymptotic quantities, can be constrained by such experiments. This observation implies that a certain combination of spectroscopic factor and single-particle wave function, essentially $\mathcal{S}_c^{1/2} u_c(r)$ at and beyond the nuclear surface, can be well constrained.

C. An alternative definition of the spectroscopic factor

When working in an R-matrix framework with channel radii, it is convenient to utilize an alternative definition of the spectroscopic factor that only depends on the wave function inside the channel radii. This property makes it very useful for

studying isospin symmetry. From a computational perspective, the alternative definition is

$$\mathbb{S}_c = \frac{\int_0^{a_c} \mathcal{R}_c^2(r)\, r^2\, dr}{\langle \tilde{\Psi}|\Psi\rangle_0^a}. \tag{72}$$

In this work, I will refer to $\mathbb{S}_c$ as the *internal* spectroscopic factor. The phenomenological replacement of the radial overlap function, analogous to Eq. (58), is

$$\frac{R_c(r)}{\left(\langle \tilde{\Psi}|\Psi\rangle_0^a\right)^{1/2}} \rightarrow \mathbb{A}_c \frac{u_c(r)}{r\left(\int_0^{a_c} u_c^2(r)\, dr\right)^{1/2}}, \tag{73}$$

where $\mathbb{A}_c$ is the internal spectroscopic amplitude and $\mathbb{S}_c = \mathbb{A}_c^2$. The quantities $\mathbb{S}_c$ and $\mathbb{A}_c$ can again be defined as real quantities when the energy is real. Now, because the normalization does not extend over all space, the internal spectroscopic factor and amplitude can be defined for a much broader class of states without approximation, including R-matrix eigenfunctions. In this framework, the analog of Eq. (67) becomes much simpler:

$$\gamma_c^2 = \mathbb{S}_c \gamma_{c,\mathrm{sp}}^2 \quad \text{or} \quad \gamma_c = \mathbb{A}_c \gamma_{c,\mathrm{sp}}. \tag{74}$$

The difference between $\mathcal{S}_c$ and $\mathbb{S}_c$ is often small, but this is not always the case, particularly when smaller channel radii are utilized and/or when the state in question has low angular momentum and lies near a channel threshold. Also note that the difference disappears for single-particle states, i.e., when $\mathcal{S}_c = \mathbb{S}_c = 1$, indicating that differences will be larger when the spectroscopic factors depart significantly from unity. It is interesting to note that Eq. (74) is how spectroscopic factors were originally defined [40,41], but this definition was largely supplanted by Eq. (54). The different definitions are alluded to in the work of Robson [37, pp. 489–490]. These differences have led to some confusion in the literature [19,42–44]. It also appears that the denominators in Eq. (67) are sometimes dropped as an approximation. It should be noted that the validity of such an approximation hinges in part on *both* the single-particle and actual reduced widths being sufficiently small.

Another consideration arises if spectroscopic factors from a shell model calculation using harmonic oscillator basis states are utilized. In this case, the energy eigenstates do not have the correct outgoing-wave behavior beyond the channel radii. Instead, the magnitude of the wave function falls off much more quickly with radius. In this case, it is likely a better approximation to consider such spectroscopic factors as *internal* spectroscopic factors $\mathbb{S}_c$ for the purpose of calculating ANCs or widths.

The distinction between $\mathcal{S}_c$ and $\mathbb{S}_c$ is closely related to the distinction between observed and formal widths or reduced widths; see the work of Descouvemont and Baye [45, Sec. 5] for definitions of these quantities. In this work, all widths are defined to be observed widths and all reduced widths to be formal reduced widths. In addition, dimensionless reduced widths are not utilized in this work. I find the proliferation of additional notation to be unnecessary and it creates additional opportunities for confusion.

V. ISOSPIN AND MIRROR SYMMETRY

Some examples of the use of isospin in the present context are provided by Refs. [36,37,46–48]. If the nuclear state B is a member of an isospin multiplet with well-defined total isospin, its decay into clusters A and a, that are also assumed to have well-defined total isospins, may be described using the isospin formalism. It is assumed that T_X are the total isospins of nuclei X, and T_{X3} are the corresponding isospin projections, where $X = B$, A, or a. One then has for the spectroscopic amplitude [33, Eq. (5.3.11), p. 193]

$$\mathcal{A}_{c'} = \langle T_A T_{A3}, T_a T_{a3} | T_B T_{B3} \rangle \tilde{\mathcal{A}}_c. \tag{75}$$

Alternatively, one can write

$$\mathbb{A}_{c'} = \langle T_A T_{A3}, T_a T_{a3} | T_B T_{B3} \rangle \tilde{\mathbb{A}}_c \tag{76}$$

or

$$\gamma_{c'} = \langle T_A T_{A3}, T_a T_{a3} | T_B T_{B3} \rangle \tilde{\gamma}_c. \tag{77}$$

Note that in general a channel c' can occur more than once in a particular nucleus. For example, a $T = 1$ $n + {}^3$H channel has both $n + {}^3$He and $p + {}^3$H analogs in the ^{4}He nucleus. Mirror channels can only occur once in the respective nuclei. In all three of the above cases, the spectroscopic amplitude or reduced width written with the tilde symbol is common to the multiplet, and the symbols on the left without the tilde vary across the multiplet, depending upon the T_{X3} values in the Clebsch-Gordan coefficient. It is assumed that the other quantum numbers needed to define the channels c and c' remain fixed across the multiplet. It should also be noted that these definitions are in general not equivalent, although the difference between the latter two is generally very small. The latter two approaches can be made exactly equivalent if an average single-particle reduced width is used for the multiplet [49,50]. In the case of an isospin mirror pair, the states have opposite T_{X3} components, resulting in spectroscopic factors (for the first two definitions) or squared reduced width amplitudes (for the third definition) that are equal.

Isospin symmetry is violated by the Coulomb interaction, which dominates beyond the channel radii. It is further broken by energy displacements, which also contribute to different radial dependences beyond the channel radii. Consequently, one expects the first approach, Eq. (75) involving normalizations that extend to infinity, to be less accurate than the second two, Eqs. (76) and (77) involving normalizations inside the channel radii [37]. Note also that the utilization of the more accurate approaches, Eqs. (76) or (77), leads to isospin symmetry breaking in the traditional spectroscopic factor defined by Eq. (75). As already discussed in Sec. IV B, it is also important to utilize channel radii just outside the nuclear surface, in order to avoid introducing additional isospin symmetry breaking.

If either of the first two approaches, defined by Eqs. (75) and (76) using spectroscopic amplitudes, are utilized in conjunction with the well-depth procedure to determine the single-particle wave functions, some additional dependence on the short-range behavior of the single-particle potential is introduced. For example, this procedure for determining the single-particle wave function includes the Thomas-Ehrman

shift [51,52] in the energy. However, if the level in question has a small spectroscopic amplitude for the single-particle configuration, this energy shift is spurious. It has also been found that nonlocal contributions to the single-particle potential are important when the spectroscopic amplitude is small [53]. One approach to minimizing this issue that has been suggested is to match the single-particle level energy by varying a surface potential rather than the main (volume) Woods-Saxon potential [54]. For the purposes of this work, the question can be bypassed by adopting the third approach, defined by Eq. (77) using the reduced width amplitude. This procedure avoids making any reference to properties of potentials or wave functions inside the channel radii and will be utilized extensively in the remainder of this work.

VI. SINGLE-LEVEL MIRROR SYMMETRY

It is very common in practice to work with cases involving mirror symmetry between isolated levels. Here, I describe two approaches to this case and provide some examples.

A. *R*-matrix approach

If there is only a single important channel, the relationship between ANCs and/or widths of the mirror states are particularly simple. Using the *R*-matrix framework and Eq. (71), the width or ANC of a level is related to the reduced width via

$$X^{-1} = \gamma^{-2} + \left(\frac{\partial \hat{\mathcal{S}}}{\partial E} \right)_a , \qquad (78)$$

where the channel label has been dropped. Assuming the value γ^2 is identical for the mirror levels in question, as implied by Eq. (77), one then finds

$$X_1^{-1} - \left(\frac{\partial \hat{\mathcal{S}}_1}{\partial E} \right)_a = X_2^{-1} - \left(\frac{\partial \hat{\mathcal{S}}_2}{\partial E} \right)_a , \qquad (79)$$

where the subscript 1 or 2 indicates the particular member of the mirror pair, keeping in mind that the states differ in both energy and charge.

The multichannel case is only slightly more complicated. According to Eq. (71), one has

$$X_c = \frac{\gamma_c^2}{1 + \sum_{c'} \gamma_{c'}^2 \left(\frac{\partial \hat{\mathcal{S}}_{c'}}{\partial E} \right)_{a_{c'}}} . \qquad (80)$$

This equation may be inverted to yield

$$\gamma_c^2 = \frac{X_c}{1 - \sum_{c'} X_{c'} \left(\frac{\partial \hat{\mathcal{S}}_{c'}}{\partial E} \right)_{a_{c'}}} . \qquad (81)$$

Suppose the widths and/or ANCs X_{1c} of a state in nucleus 1 are known. The procedure is to determine corresponding widths and/or ANCs X_{2c} of the mirror state 2 is as follows. First, the X_{1c} are converted into γ_c using Eq. (81). Then the γ_c are converted to X_{2c} using Eq. (80), implicitly assuming the reduced widths γ_c are equal for both states. The result of this procedure is

$$X_{2c} = \frac{X_{1c}}{1 + \sum_{c'} X_{1c'} \left[\left(\frac{\partial \hat{\mathcal{S}}_{2c'}}{\partial E} \right) - \left(\frac{\partial \hat{\mathcal{S}}_{1c'}}{\partial E} \right) \right]_{a_{c'}}} . \qquad (82)$$

B. Result of Timofeyuk and collaborators

Another formula relating ANCs and/or widths of mirror states has been put forward by Timofeyuk and collaborators [26,32,55–57]. It only considers a single channel and in the present notation reads

$$\frac{X_1 / |\mathcal{O}_1(a)|^2}{X_2 / |\mathcal{O}_2(a)|^2} = \left| \frac{\exp(i\sigma_1) \, F_1(\tilde{a}) / k_1}{\exp(i\sigma_2) \, F_2(\tilde{a}) / k_2} \right|^2 . \qquad (83)$$

Here, the quantity $\tilde{a}$ is a channel radius, but it need not be the same as a. The left side of this equation is essentially a ratio of ANCs and/or widths and the right side is a prediction. This formula is nontrivially different from Eq. (79), that does not involve the regular Coulomb function or predict the relationship to be a ratio. As discussed in Refs. [26,57], the derivation of this formula depends on certain assumptions about the wave functions and matrix elements of the Coulomb interaction in the nuclear interior.

Some insight into this equation can be deduced in the *R*-matrix framework by making some assumptions regarding Eqs. (32) and (41), for $r \leqslant \tilde{a}$:

$$\frac{F_1(r)}{F_1(\tilde{a})} = \frac{F_2(r)}{F_2(\tilde{a})} , \qquad (84a)$$

$$[V(r) + V_C(r) - V_{pC}(r)]_1 = [V(r) + V_C(r) - V_{pC}(r)]_2 , \qquad (84b)$$

$$u_1(r) = u_2(r), \quad \text{and} \qquad (84c)$$

$$b = a = \tilde{a} . \qquad (84d)$$

Note that $u_1(r) = u_2(r)$ embodies the mirror-symmetry assumption and implies the single-particle reduced widths are equal. The assumption that $b = a$ implies that the channel radius is large enough such that at the channel radius, Coulomb interactions are negligible and the unmodified Coulomb functions can be utilized. In Eq. (41), I further assume the unbound state is well below the Coulomb and angular momentum barriers such that $G(a) \gg F(a)$ and the left-hand side of the equation may be replaced by $u(a)[P(a)/(ka)]^{1/2}$. Then, Eq. (32) (for a bound state) and Eq. (41) (for an unbound state) both lead to

$$\gamma_{\mathrm{sp}}^2 = \frac{2\mu |O(a)|^2}{\hbar^2 a} \left| \frac{\exp(i\sigma)}{k} \int_0^a F(V + V_C - V_{pC}) u \, dr \right|^2 . \qquad (85)$$

Considering the assumptions described by Eq. (84) and assuming equal internal spectroscopic factors described by Eq. (74), the quantity

$$\left| O(a) F(a) \frac{\exp(i\sigma)}{k} \right|^2 \qquad (86)$$

should be equal for both members of the mirror pair. If this is true, then Eq. (83) reduces to $X_1 = X_2$, which is equivalent to Eq. (79), *if* the volume renormalization factors $\partial \hat{\mathcal{S}} / \partial E$ are neglected. In fact, Timofeyuk and Descouvemont [56] point out that Eq. (83) should be modified by the volume renormalization factor for the case of an unbound state. However, they mention no such correction for bound states, although it is clear that it should be included in this case as well.

A mathematical explanation of why the quantity given by Eq. (86) is approximately equal for both members is

provided by the Wentzel-Kramers-Brillouin (WKB) approximation [58]. For bound states, or unbound states below the Coulomb and/or angular momentum barriers, the solutions to Eq. (1) for radii beyond the range of the nuclear potential depend exponentially on the radius. Following Ref. [58, Eqs. (34.4), (34.5), and (34.8), pp. 270–271],

$$u_\pm \propto \kappa^{-1/2} \exp\left(\pm \int \kappa\, dr\right) \quad \text{with} \tag{87a}$$

$$\kappa = \left\{ \frac{2\mu}{\hbar^2}\left[-E + \frac{\hbar^2}{2\mu}\frac{\ell(\ell+1)}{r^2} + V_c(r) \right] \right\}^{1/2}, \tag{87b}$$

where κ is real. One also finds

$$\frac{1}{u_\pm}\frac{du_\pm}{dr} = -\frac{1}{2\kappa}\frac{d\kappa}{dr} \pm \kappa \tag{88}$$

for the logarithmic derivative. For the energy regime under consideration, the regular Coulomb function F is identified as the exponentially increasing solution and the outgoing Coulomb function O as the exponentially decreasing solution. One thus has

$$\frac{1}{F}\frac{dF}{dr} \approx \left(\frac{1}{u_+}\frac{du_+}{dr}\right)_{\text{WKB}} = -\frac{1}{2\kappa}\frac{d\kappa}{dr} + \kappa \quad \text{and} \tag{89a}$$

$$\frac{1}{O}\frac{dO}{dr} \approx \left(\frac{1}{u_-}\frac{du_-}{dr}\right)_{\text{WKB}} = -\frac{1}{2\kappa}\frac{d\kappa}{dr} - \kappa. \tag{89b}$$

I note in passing that this result for the WKB shift function

$$\hat{S}_{\text{WKB}} = \left(\frac{r}{u_-}\frac{du_-}{dr}\right)_{\text{WKB}} = -\frac{r}{2\kappa}\frac{d\kappa}{dr} - \kappa r \tag{90}$$

agrees with that given in Lane and Thomas [3, Eq. (A.18), p. 350], apart from their Langer modification. As discussed in Ref. [3], this expression may also be used to derive a WKB approximation for the energy derivative of the shift function. The Wronskian relation, Eq. (3), may be written as

$$\frac{1}{F}\frac{dF}{dr} - \frac{1}{O}\frac{dO}{dr} = \frac{k}{FO\exp(i\sigma)}. \tag{91}$$

Thus, in the WKB approximation,

$$\left| O(a)F(a)\frac{\exp(i\sigma)}{k} \right|_{\text{WKB}} = \frac{1}{2\kappa}. \tag{92}$$

One is now in a position to understand why this quantity will be approximately the same for mirror states. Considering Eq. (1) and the approximation given by Eq. (84c) at $r = a$, one finds

$$E_2 - E_1 \approx V_{C2}(a) - V_{C1}(a) \tag{93}$$

for the Coulomb energy difference of the single-particle wave functions. Then considering Eq. (87b), one has $\kappa_1(a) \approx \kappa_2(a)$, and one does indeed find Eq. (92) to be the same for both states of the mirror pair. It is important to note that the Coulomb energy difference plays a key role in this approximate equivalence and that of Eqs. (79) and (83). A somewhat similar analysis of the justification for Eq. (83) has been given in Ref. [57].

C. Discussion

Four methods for implementing mirror symmetry have been introduced. Three of the methods are based on Eqs. (75)–(77); the fourth is described in the previous subsection. The R-matrix approach based on Eq. (77) is described in detail in Sec. VI A. Of all of the approaches, this one most strongly adopts the spirit of the phenomenological R matrix, as no assumptions about potentials or wave functions inside the channel radii are necessary. Approaches based upon Eq. (75) are expected to be somewhat less accurate than the others, because this spectroscopic amplitude is normalized over all space, which unnecessarily includes isospin violation due to the Coulomb force beyond the channel radii. Using the internal spectroscopic amplitude, as defined by Eq. (76), does not suffer from this shortcoming. It can also supply some internal mirror symmetry breaking due to mirror symmetry breaking in the single-particle reduced-width amplitudes. The R-matrix approaches, Eqs. (76) or (77), also have the advantage of allowing multichannel effects to be included. It is not clear from this discussion which approach, Eqs. (76) or (77), is preferable. It may be possible to address this question in particular cases if accurate many-body calculations are available. I have some preference for Eq. (77), due to its conceptual simplicity.

The approach of Timofeyuk described in Sec. VI B leads to results that are similar to the other methods in most cases. However, this formula does not take into account the volume renormalization factors, which can lead to a significant error if these factors differ significantly from unity. This consideration is particularly relevant for the first excited $1/2^+$ states of ^{13}C and ^{13}N discussed below.

D. Examples

1. $\ell = 0$ mirror states in ^{13}C and ^{13}N

The first excited $1/2^+$ states of ^{13}C and ^{13}N have long been a testing ground for mirror symmetry [49,51,56]. The level is single particle in nature and is bound in ^{13}C but unbound in ^{13}N. The neutron ANC in ^{13}C has been measured by two independent groups using the ^{12}C$(d, p)^{13}$C transfer reaction in similar kinematics. Liu *et al.* [59] measured $C_n^2 = 3.39 \pm 0.59$ (stat + sys) fm^{-1}, while Imai *et al.* [60] reported $C_n^2 = 3.65 \pm 0.34$ (stat) ± 0.35 (sys) fm^{-1}. In neither experiment is it clear if the systematic uncertainty includes the theoretical uncertainty from the transfer reaction analysis; I adopt $C_n^2 = 3.52 \pm 0.50$ fm^{-1}. The proton width in ^{13}C is taken from the elastic scattering data and R-matrix analysis of Meyer *et al.* [11]. This work does not quote uncertainties; I adopt $\Gamma_p = 33.8 \pm 2.0$ keV, which is also consistent with the analysis of Ref. [49].

First, calculations were performed using two-body potential and assuming spectroscopic factors of unity. The potential depth was adjusted separately for each state to reproduce the known separation energy. With the standard potential parameters given in Sec. II F, the depths for each state only difference by a few percent. Likewise, the single-particle reduced widths for each state only differed by a few percent. The resulting ANC and proton width are shown as the filled circle in Fig. 6. Then the potential was fixed at a depth taken to be the average
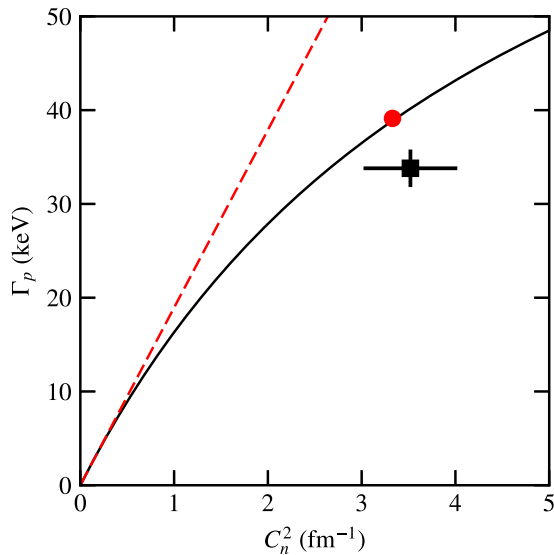
FIG. 6. The relationship between Γ_p and C_n^2 for the first excited states of ^{13}C and ^{13}N. The solid and dashed curves show the results of Eqs. (79) and (83), respectively. The filled circle shows the results of the single-particle calculation. The filled square indicates the experimental results.

FIG. 8. The relationship between C_p^2 and C_n^2 for the first excited states of ^{17}O and ^{17}F. The solid and dashed curves show the results of Eqs. (79) and (83), respectively. The filled circle shows the results of the single-particle calculation. The filled square indicates the experimental results.

two results found for each state. The relationship predicted for Γ_p versus C_n^2 using Eq. (79), taking the common γ^2 to be a varying parameter, is shown as the solid curve in Fig. 6. The curve shows significant curvature, due to volume renormalization factors that depend upon $\partial\hat{\mathcal{S}}/\partial E$. The experimental results are shown as the filled square with error bars, which are in fair agreement with the solid curve.

The sensitivity of Eq. (79) to the channel radius is shown as the solid curve in Fig. 7, for $C_n^2 = 3.52$ fm^{-1}. This sensitivity is seen to be rather modest. Equation (79) is insensitive to the tail of the nuclear potential: $\pm10\%$ changes in r_n only change the solid curve by 1%. Such changes do of course modify the single-particle ANC and width more significantly. The effect of ignoring the tail of nuclear potential completely is shown as the dashed curve. This insensitivity indicates that
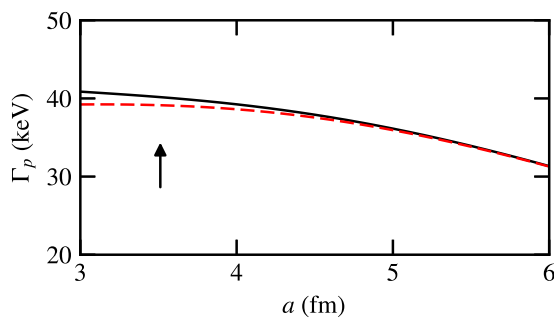
the tail of the nuclear potential could be safely ignored for this calculation.

The prediction of Eq. (83) assuming the same channel radius is shown by the dashed curve in Fig. 6. For larger values of C_n^2 and Γ_p, it is seen to diverge significantly from the solid curve given by Eq. (79), the single-particle values, and the experimental measurements. The disagreement between Eq. (83) and the single-particle model, microscopic models, and experiment has been noted previously [26,32,56]. If volume renormalization factors in Eq. (79) are neglected, the result from that equation becomes very close to that Eq. (83). I thus conclude that the disagreement between Eq. (83) and other approaches and experiment is due to the lack of volume renormalization factors in Eq. (83), a deficiency that has already been noted.

2. $\ell = 0$ mirror states in ^{17}O and ^{17}F

The situation with the first excited $1/2^+$ states of ^{17}O and ^{17}F is quite similar to the previous example. The states are single particle in nature, but in this case both states are bound. The neutron ANC in ^{17}O has been determined by the analysis of ^{16}O(d, p) data by Guo *et al.* [61] to be $C_n^2 = 8.4 \pm 1.3$ fm^{-1}. The proton ANC in ^{17}F has been reviewed by Artemov *et al.* [62], where their own and previous proton transfer experiments were analyzed to yield $C_p^2 = 6220 \pm 780$ fm^{-1}. The proton ANC was also determined using ^{16}O$(^3$He$, d)$ by Gagliardi *et al.* [63] to be $C_p^2 = 6490 \pm 680$ fm^{-1}. I adopt $C_p^2 = 6380 \pm 510$ fm^{-1}, which is also in the range required to correctly describe low-energy ^{16}O(p, γ) cross-section measurements to the first excited state of ^{17}F [61,64,65].

Calculations were performed in the same manner as in the previous example and are shown in Fig. 8. In this case, the prediction of Eq. (79) does not deviate so much from that of

FIG. 7. The relationship between Γ_p and the channel radius predicted by Eq. (79) for a fixed value of C_n^2. The solid and dashed curves show the results of including and ignoring the tail of the nuclear potential, respectively. The arrow indicates the nominal channel radius of 3.51 fm used for the calculations shown in Fig. 6 and discussed in the text.
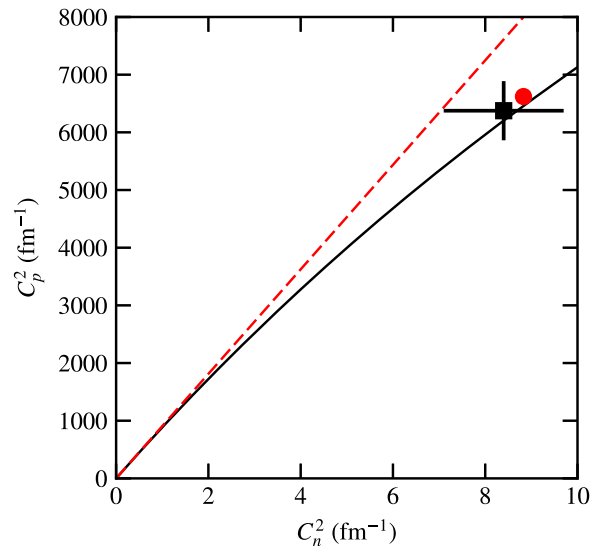
Eq. (83). This finding results because this case is more tightly bound and has a higher charge, leading to a smaller effect from the volume renormalization factors. Both calculations are in reasonable agreement with the experimental results.

For this case, it has been noted by Refs. [55,66,67] that Eq. (83) is not in good agreement with calculations using the single-particle model or other more sophisticated models. Possible explanations, such as core excitations, are discussed in these works. However, the inclusion of the volume renormalization factors brings Eq. (83) into much better agreement with the other models. This appears to be the primary reason for the discrepancy.

3. $\ell = 0$ mirror states in ^{27}Al and ^{27}Si

The $9/2^+$ mirror pair located at $E_x = 7807$ keV in ^{27}Al and 7590 keV in ^{27}Si couple to a nucleon and ^{26}Al with $\ell = 0$, but with a small spectroscopic factor of about 0.01. This situation thus provides an example in a regime where the levels in question are not close to being single-particle states. Two independent measurements of the ^{26}Al(d, p) reaction are described in Refs. [68–71]. Using the reported spectroscopic factors and neutron binding potentials, the $\ell = 0$ ANC value from Ref. [68] is $C_n^2 = 0.301 \pm 0.062$ fm^{-1}, where the error includes the experimental uncertainty and a 15% uncertainty from the transfer reaction analysis. Similarly, Refs. [69,70] yield $C_n^2 = 0.259 \pm 0.053$ fm^{-1}, where the error includes the experimental uncertainty only. Since both experiments were performed with similar kinematics and utilized nearly identical transfer reaction analyses, a common systematic error of 15% from the transfer reaction analysis is assumed for both experiments, leading to an adopted value of $C_n^2 = 0.284 \pm 0.054$ fm^{-1}. The mirror level is unbound in ^{27}Si, appearing as a resonance at $E_R = 126.8 \pm 0.9$ keV. Since $\Gamma_p \ll \Gamma_\gamma$ for this resonance, its strength is governed by Γ_p which can be estimated from C_n^2 of the mirror state. This procedure has been carried out in Refs. [68–70], where it is found that this resonance dominates the ^{26}Al(p, γ) reaction rate for temperatures relevant to asymptotic giant branch and Wolf-Rayet stars. The adopted resonance energy is determined from the excitation energy measured by Lotay *et al.* [13] and the proton separation energy from Ref. [14]. Because the resonance is far below the Coulomb barrier, the calculated Γ_p is quite sensitive to the energy: The 0.9-keV uncertainty contributes a 13% uncertainty to the Γ_p deduced using mirror symmetry. Note also that this uncertainty in the resonance energy contributes a further *correlated* uncertainty in the thermonuclear reaction rate.

Although these levels can couple to $\ell = 2$ nucleons, the contributions of these channels negligibly effect the volume renormalization factors and are neglected. Because of the small $\ell = 0$ spectroscopic factor, the volume renormalization factor is likewise small, leading to a linear proportionality between Γ_p and C_n^2 in all approaches. Note, however, that this factor cannot be neglected when calculating single-particle ANCs or widths. The predicted relation assuming equal reduced-width amplitudes, Eq. (79), is shown by the solid curve in Fig. 9. This case has significant mirror symmetry breaking in the single-particle reduced width amplitudes:
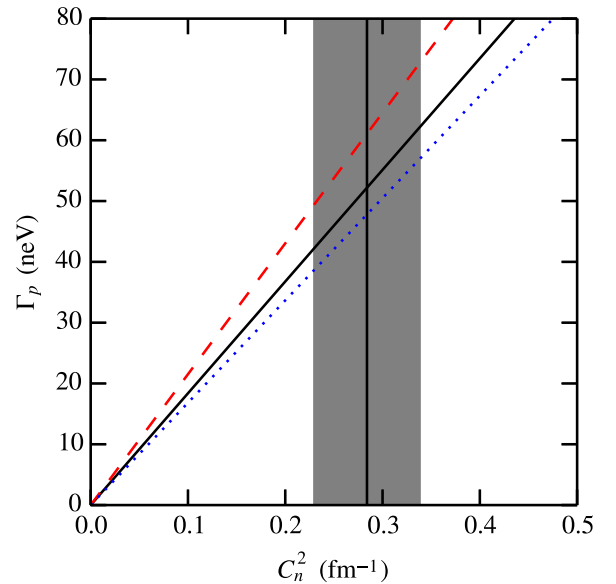

FIG. 9. The relationship between C_n^2 and Γ_p for the 7807- and 7590-keV $9/2^+$ states of ^{27}Al and ^{27}Si. The solid, red-dashed, and blue-dotted curves show the results of Eq. (79); Eq. (74); and Eqs. (59) and (60), respectively. The vertical line and gray error band show the adopted experimental C_n^2 value.

$\gamma_{n,\mathrm{sp}}^2 = 2.10$ MeV and $\gamma_{p,\mathrm{sp}}^2 = 2.46$ MeV, a 17% difference. Assuming a constant *internal* spectroscopic factor and using Eq. (74) thus lead to a somewhat different prediction, shown by the red-dashed line. The approach of Timofeyuk and collaborators, using the same channel radius as in the other approaches, is not shown but is very close to the red-dashed line. Some previous analyses have assumed that the traditional spectroscopic factor is the same for both states, and related Γ_p and C_n^2 using Eqs. (59) and (60). As discussed in Sec. V, this approach is expected to be somewhat less accurate than the other two shown in Fig. 9. This prediction is shown by the blue-dotted curve, where it is seen to lie somewhat below the other two. The adopted experimental value for C_n^2 is shown by the vertical line and gray error band. All of the approaches are in reasonable overall agreement and the interpretation of the experimental data is not seriously limited by the choice of model. Considering Eqs. (79) and (74), the solid-black and red-dashed curves, a value of $\Gamma_p = 57 \pm 15$ neV is extracted, in agreement with previous determinations [68–70]. Note also that any deviation of a prediction from the blue-dotted curve can be interpreted as a renormalization of the traditional spectroscopic factor between the mirror states.

VII. MULTILEVEL MIRROR SYMMETRY

It is important to note that all of the definitions of bound or unbound resonant energy levels discussed up to this point violate isospin. This occurs because the resonance condition, which is always some version on an outgoing-wave boundary condition, depends upon the energy and charges in the external region. Since isospin rotations generally involve both changes in charge and energy shifts, this situation is both

necessary and expected. In the R-matrix case, the resonance condition is given by Eq. (57), which requires the logarithmic derivative match the shift function at the channel radius. The symmetry breaking coming from the boundary condition has important effects if one considers isospin transformations on a set of levels with the same spin and parity. An R-matrix approach to calculating the effects arising from this symmetry breaking is given below for the case of mirror symmetry, along with an example application to 2^+ states in ^{18}O and ^{18}Ne.

A. General phenomenological approach

For examples of the use of isospin in multilevel phenomenological R-matrix analyses, one may see Refs. [46,48] for light nuclei and Ref. [37] for heavier nuclei. It is very useful to work in a basis that satisfies boundary conditions that are independent of energy and isospin. The energy-independent boundary conditions of traditional R-matrix theory [3,72] provide an ideal basis for this purpose. For these states, the logarithmic derivatives at the channel radius are equal to the constants B_c, rather than the energy- and charge-dependent shift function of the resonance boundary conditions given by Eq. (57). Note also that any tail of the nuclear potential must be kept independent of energy (i.e., fixed) in an R-matrix calculation.

I will consider the transformation from a set of resonance levels of particular J^π in nucleus 1 to a mirror nucleus 2. A set of states $\{E_i(1), \gamma_{ic}(1)\}$ satisfying resonance boundary conditions in nucleus 1 may be transformed into a set $\{\hat{E}_\lambda(1), \hat{\gamma}_{\lambda c}(1), B_c\}$ satisfying constant boundary conditions as described in Appendix B. The number of levels is preserved by the transformation. I next suppose that the difference between the Hamiltonians of the nuclei is $\Delta H = H_2 - H_1$. Using the internal basis states $|\lambda\rangle$ solving H_1 with boundary conditions B_c, the level matrix [3, IX.1, Eq. (1.11), p. 294] for nucleus 2 may be written as

$$[A^{-1}]_{\lambda\mu} = (\hat{E}_\lambda(1) - E)\delta_{\lambda\mu} + \langle\lambda|\Delta H|\mu\rangle$$
$$- \sum_c \hat{\gamma}_{\lambda c}(1)\hat{\gamma}_{\mu c}(1)(\hat{\mathcal{S}}_c + i\mathcal{P}_c - B_c), \quad (94)$$

where shift and penetration factors are evaluated for the energy E in nucleus 2 and at the channel radii. This equation results from applying Eqs. (58)–(60) of Lane and Robson [17]; see also Ref. [48]. If the internal matrix elements $\langle\lambda|\Delta H|\mu\rangle$ could be evaluated, this equation could be put into standard form by diagonalization and the R-matrix parameters for nucleus 2 would be determined. In a phenomenological analysis, this avenue is unavailable. The operator ΔH consists of Coulomb potentials and possibly charge-symmetry violating nuclear interactions. It is expected that the dominant contribution to $\langle\lambda|\Delta H|\mu\rangle$ will be a constant Coulomb energy shift along the diagonal, with variations along the diagonal and off-diagonal elements being much smaller. I thus assume that $\langle\lambda|\Delta H|\mu\rangle = \Delta_\lambda \delta_{\lambda\mu}$. In this case, no diagonalization is necessary and the R-matrix parameters for nucleus 2 are

$$\hat{E}_\lambda(2) = \hat{E}_\lambda(1) + \Delta_\lambda \quad \text{and} \quad (95a)$$

$$\hat{\gamma}_{\lambda c}(2) = \pm\hat{\gamma}_{\lambda c}(1). \quad (95b)$$

TABLE II. Adopted information for the first three 2^+ states of ^{18}O and ^{18}Ne.

	^{18}O		^{18}Ne	
$n\ell_j$	E_x (keV)	C_c^2 (fm^{-1})	E_x (keV)	C_c^2 or Γ_c (fm^{-1} or keV)
$2s_{1/2}$	1982.1	5.77 ± 0.63	1887.3	16.0 ± 8.0
$1d_{5/2}$		2.10 ± 0.23		2.6 ± 1.2
$2s_{1/2}$	3920.4	4.11 ± 0.62	3616.4	148 ± 56
$1d_{5/2}$		0.45 ± 0.06		3.1 ± 1.2
$2s_{1/2}$	5254.8	2.18 ± 0.33	5098 ± 8	44.5 ± 1.7
$1d_{5/2}$		0.0080		

I will usually assume constant $\Delta_\lambda = \Delta$, but allowing the diagonal elements to vary provides the flexibility needed to exactly match the resonance energies in nucleus 2 to experimental values, if desired. The sign in Eq. (95b) is chosen to be consistent with Eq. (77), which predicts that mirror reduced widths will at most differ by a change in sign. Finally, the level parameters $\{\hat{E}_\lambda(2), \hat{\gamma}_{\lambda c}(2), B_c\}$ may be transformed into resonance parameters for nucleus 2, $\{E_i(2), \gamma_{ic}(2)\}$, using the method described in Appendix B. For $\Delta_\lambda = \Delta$, this procedure is independent of the B_c values used.

These procedures produce energy shifts of the resonance levels in mirror nuclei in addition to the Δ_λ. The additional changes arise from the differences in the external wave functions (i.e., coupling to the continuum). These shifts are the multilevel generalization of the well-known Thomas-Ehrman shift [51,52]. In addition, a particular reduced width amplitude $\gamma_{ic}(2)$ has in general a parentage in *all* of the $\gamma_{jc}(1)$. This mixing leads to a breaking of the simple single-level isospin relation, Eq. (77), for the resonant reduced width amplitudes. In the multilevel case, this equation should applied instead to the reduced width amplitudes of the states satisfying energy- and isospin-independent boundary conditions.

B. Application to 2^+ states in ^{18}O and ^{18}Ne

The mirror nuclei ^{18}O and ^{18}Ne have three 2^+ states with significant spectroscopic strength in nucleon decay channels that are located near the nucleon separation threshold (particularly in the case of ^{18}Ne). This system thus provides a good case for demonstrating the nontrivial effects that may arise. The importance of continuum mixing in this case has been noted and studied previously using the shell model embedded in the continuum [73,74]. The ANC of the second 2^+ state in ^{18}Ne plays an important role in determining the rate of the ^{17}F(p, γ)^{18}Ne reaction in novae [73,75,76]. The notation (1) and (2) will often be utilized to indicate ^{18}O and ^{18}Ne in this subsection.

The available information for the excitation energies and widths or ANCs for these states is summarized in Table II. The excitation energies are very well known, with the exception of the 2_3^+ state of ^{18}Ne, where the value adopted is the weighted average of 5075 ± 13 keV [77], 5099 ± 10 keV [77], and 5106 ± 8 keV [78], with the error rescaled to provide a χ^2 of 2. The ^{17}O$+n$ ANCs for the 2_1^+ and 2_2^+ states of ^{18}O

are taken from Al-Abdullah *et al.* [75], who performed an analysis of their ^{13}C(^{17}O, ^{18}O)^{12}C data and the ^{17}O(d, p)^{18}O data of Li *et al.* [79]. The $2s_{1/2}$ ANC for the 2_3^+ state of ^{18}O is calculated from the spectroscopic factor and binding potential reported by Ref. [79]. The value was renormalized downward by 10%, a factor the brought the ANCs of Ref. [79] into agreement with Ref. [75] for the 2_1^+ and 2_2^+ states. The experimental ^{17}O(d, p)^{18}O angular distribution indicates that the $1d_{5/2}$ spectroscopic factor for the 2_3^+ state of ^{18}O is very small [79]. This finding is supported by the shell model calculations of Lawson *et al.* [80]. The ANC for the state adopted in Table II is based on their calculations; setting this quantity to zero does not significantly change any of the results reported below. The ANCs for the 2_1^+ and 2_2^+ states of ^{18}Ne are taken from the measurements of Kuvin *et al.* [76]. Note that this is a difficult radioactive ion beam experiment with limited angular coverage. The $2s_{1/2}$ and $1d_{5/2}$ ANCs were not independently determined; the ratio from the mirror nucleus was assumed. As shown in the table, the uncertainties in the ANCs are rather large and are the result of adding the experimental statistical and systematic uncertainties reported in Ref. [76] in quadrature. The proton width of the 2_3^+ state of ^{18}Ne is determined from the weighted average of 45 ± 5 keV [78], 45 ± 2 keV [81], and 42 ± 4 keV [82]. The result of Hahn *et al.* [78] is a total width determination and the latter two were extracted from fits to elastic scattering that appear to have assumed the width is entirely due to $\ell = 0$ proton emission to the ^{17}F ground state. The $1d_{5/2}$ single-particle width for this state is 6.6 keV, so it is potentially possible that this channel contributes somewhat to the total width. However, in light of the small spectroscopic factor for this channel in the mirror state, this is unlikely. I also note that Almaraz-Calderon *et al.* [83] report $\Gamma_{p'}/\Gamma_p = 0.11 \pm 0.04$ for a combination of the 5.10- and 5.15-MeV states of ^{18}Ne. The decay of a 2^+ state to a proton and the first excited state of ^{17}F requires $\ell = 2$. Considering the additional Coulomb barrier present in this case, this reported branch to the first excited state of ^{17}F cannot involve the 2^+ state of ^{18}Ne. For these reasons, the measured proton width is assigned entirely to the $2s_{1/2}$ channel.

I first investigated the results of treating the levels independently, using two different methods, as shown in Table III. Al-Abdullah *et al.* [75] predicted ANCs in ^{18}Ne from the experimental values for ^{18}O, assuming the spectroscopic factors $\mathcal{S}_c$ are the same for both members of the mirror pair, using Eq. (59). I have used the same approach for the ANCs or widths [using Eq. (60)], with the results shown in the fourth column. These findings are in good agreement with their work for the first two levels, the only 2^+ states analyzed in Ref. [75]. For the remainder of the calculations shown in this subsection, the depth of the Woods-Saxon potential was fixed at 53.5 MeV, which places the $\ell = 0$ single-particle states at -4.03 and -0.48 MeV relative to the nucleon separation thresholds in ^{18}O and ^{18}Ne, respectively. The fifth column shows the results of applying Eq. (82) to determine the ANCs or widths. Little difference is seen, except for the Γ_p for the 2_3^+ state, which is about 30% larger in the latter approach. The single-particle width of this state is rather broad, about 330 keV, which is the likely reason for some of the difference in this

TABLE III. The quantities ℓ, $E_i(1)$, and $E_i(2)$ are the nucleon orbital angular momentum and the experimental level energies relative to the nucleon separation thresholds in ^{18}O and ^{18}Ne, respectively. The final two columns provide the ANC or width predictions in ^{18}Ne, treating each pair of levels independently and using two different methods.

	^{18}O	^{18}Ne		
	$E_i(1)$	$E_i(2)$	Eqs. (59) and (60) C_c^2 or Γ_c	Eq. (82) C_c^2 or Γ_c
ℓ	(MeV)	(MeV)	(fm^{-1} or keV)	(fm^{-1} or keV)
0	-6.062	-2.034	14.89	14.87
2			2.84	2.59
0	-4.124	-0.305	117.4	125.2
2			2.48	2.20
0	-2.790	1.176	102	130
2			1.9×10^{-2}	1.7×10^{-2}

case. There is also little sensitivity to the assumed nuclear potential: Neglecting it entirely changes the results by less than 10%, for the preferred channel radius of 3.86 fm. This value corresponds to $a = R_n + a_n$, as discussed in Sec. II F, and lies just outside the nuclear surface, such that additional mirror symmetry breaking is avoided. This sensitivity to the tail of the nuclear potential and channel radius are shown in Fig. 10. For the 2_1^+ and 2_2^+ states, the predicted ANCs in ^{18}Ne are in good agreement with the experimental values of Kuvin *et al.* [76] shown in Table II, although the large experimental errors preclude any accurate statement. However, for the 2_3^+ state, the predicted proton widths are more than a factor of 2 larger than the accurately known experimental value. The calculations using Eq. (82) included the $\ell = 2^*$ channel introduced below, using the $\gamma_{ic}(1)$ from Table IV. This consideration had very little effect.

In this case, there are three important channels with thresholds located in the neighborhood of the first three 2^+ levels. The first two are the $\ell = 0$ and $\ell = 2$ $n + {}^{17}$O or $p + {}^{17}$F channels already discussed. The nuclei ^{17}O and ^{17}F have low-lying $1/2^+$ states, thus leading to an additional important channel and couples $\ell = 2$ nucleons to these excited states. These channels will be indicated as $\ell = 2^*$. No experimental information for these channels is available. In addition, the relative signs of the reduced width amplitudes within a particular channel have a significant impact in the transformation process described in Appendix B. These unknown parameters can be fixed using the shell model. In a simple shell model picture for the 2^+ states, with two $T = 1$ nucleons outside an ^{16}O core, both the $\ell = 0$ and $\ell = 2^*$ channels arise from the $(d_{5/2}, s_{1/2})$ component of the wave function. This consideration leads to the spectroscopic amplitudes being equal, up to an overall sign that is irrelevant in the present case. More detailed calculations were performed using the code NUSHELLX [84], with the Zuker-Buck-McGrory (ZBM) model space and interactions for nucleons outside a ^{12}C core [85]. Both interactions given by ZBM were utilized. For the first three 2^+ states, the ratio of the $\ell = 2^*$ to $\ell = 0$ spectroscopic amplitude was always found to lie between 0.96 and 0.88,
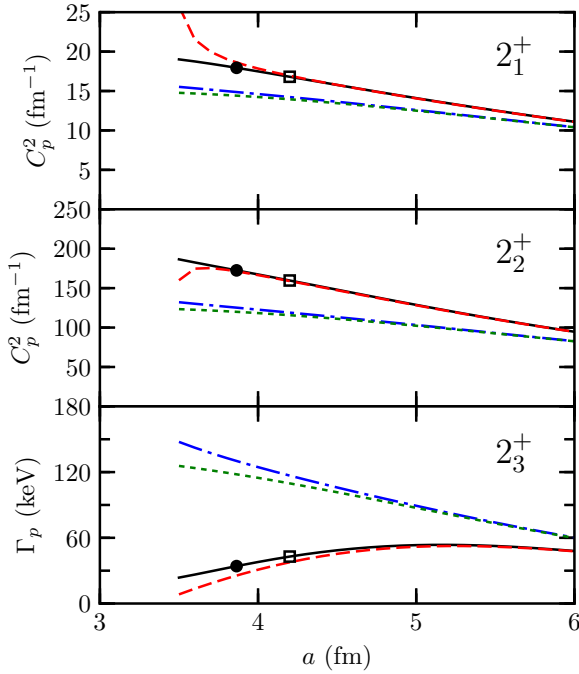
FIG. 10. Predicted $\ell = 0$ ANCs or widths for the first three 2^+ states in ^{18}Ne versus channel radius for various approaches. The results for treating the levels independently, using Eq. (82), are shown for the tail of the nuclear potential included (excluded) by the blue dash-dotted (green dotted) curve. The results for treating the levels simultaneously are shown for the tail of the nuclear potential included (excluded) by the solid black (red dashed) curve. The plotted points show the results for the simultaneous treatment with the tail of the nuclear potential included, for the preferred channel radius of 3.86 fm used for the calculations shown in Table IV (solid circles) and for a channel radius of 4.2 fm (open squares).

depending somewhat upon the particular state and interaction. The simple picture is thus confirmed within a good degree of accuracy and will be used below to estimate the parameters for the $\ell = 2^*$ channels. This calculation also predicts the signs for all of the channels, where good agreement is seen for both interactions and also the three calculations of

Lawson *et al.* [80, Table IV]. The lone exception is for the $\ell = 2$ channel for the 2^+_3 state, where the spectroscopic amplitude is very small. In this case, the sign from Ref. [80] is utilized, although it has no impact on the results reported below.

The three states are then treated simultaneously as described in Sec. VII A. The reduced width amplitudes $\gamma_{ic}(1)$ in ^{18}O were determined from the experimental ^{18}O ANCs in Table II using Eq. (81). The relative signs of the reduced width amplitudes within a particular channel have a significant impact on the transformation process described in Appendix B. These signs are taken from the shell model calculations described above. Further following the shell model, the $\ell = 2^*$ reduced-width amplitudes were adjusted such that $\hat{\gamma}_{\lambda, \ell = 2^*} = 0.815 \hat{\gamma}_{\lambda, \ell = 0}$, where 0.815 is the ratio of single-particle reduced-width amplitudes. The boundary-condition constants B_c were chosen to equal to the shift function for the 2^+_2 state in ^{18}Ne. The parameters $\{E_i(1), \gamma_{ic}(1)\}$ are then transformed to $\{\hat{E}_{\lambda c}(1), \hat{\gamma}_{\lambda c} B_c\}$. A constant shift $\Delta = 4.777$ MeV was used in Eq. (95a), to match exactly $E_2(2)$ to the experimental energy of the 2^+_2 state. The $\hat{\gamma}_{\lambda c}$ do not change sign for this mirror transformation. Then the parameters $\{\hat{E}_{\lambda c}(2), \hat{\gamma}_{\lambda c} B_c\}$ are transformed to $\{E_i(2), \gamma_{ic}(2)\}$, the resonance parameters in ^{18}Ne. Finally, the ANCs or widths are calculated from the resonance parameters using Eq. (80). Since the calculated $E_i(2)$ do not necessarily exactly match the experimental values, the experimental energy values are used in this last step. The resulting ANCs or widths and the parameter values at the steps of this process are shown in Table IV.

Significant differences are seen compared to the results considering each level independently. The squares of the ANCs of the first two 2^+ states in ^{18}Ne are predicted to be significantly larger by the multilevel calculation. This result is still in agreement with the experimental result, due to the large experimental error. In addition, the width of the 2^+_3 state is found to be about a factor of 3 smaller, such that the prediction is now below the experimental value. These finding were found to be sensitive to several ingredients in the calculation. The dominant sensitivity is to the $\ell = 0$ reduced-width amplitudes and their signs, but the $\ell = 2$ and $\ell = 2^*$

TABLE IV. Transformation of the ^{18}O (1) resonance parameters to ^{18}Ne (2) resonance parameters. The meaning of the various quantities is described in the text. The final column gives the resulting ANCs or widths in ^{18}Ne.

ℓ	$E_i(1)$ (MeV)	$\gamma_{ic}(1)$ (MeV$^{1/2}$)	$\hat{E}_\lambda(1)$ (MeV)	$\hat{\gamma}_{\lambda c}$ (MeV$^{1/2}$)	$\hat{E}_\lambda(2)$ (MeV)	$E_i(2)$ (MeV)	$\gamma_{ic}(2)$ (MeV$^{1/2}$)	C_c^2 or Γ_c (2) (fm^{-1} or keV)
0	−6.062	−0.747	−8.099	−0.999	−3.322	−2.023	−0.835	17.94
2		−1.483		−1.420			−1.494	2.53
2*		−0.609		−0.814			−0.681	0.68
0	−4.124	0.896	−5.083	1.158	−0.305	−0.305	1.158	172.5
2		−1.185		−1.343			−1.343	2.34
2*		0.730		0.944			0.944	0.48
0	−2.790	−0.789	−2.798	−0.782	1.979	1.594	−0.343	34.2
2		0.075		0.075			0.113	5.2×10^{-2}
2*		−0.643		−0.637			−0.280	1.6×10^{-2}

channels also contribute nontrivially. Changing the sign of the input $\ell = 0$ 2_2^+ reduced-width amplitude causes the predicted ANC of the 2_2^+ state in ^{18}Ne to be *smaller* than that found when the levels are considered independently. It also is found that all of the first three 2^+ states play an important role in this mixing.

Several other factors were investigated that had little influence on these results. A background level with physically reasonable reduced-width parameters placed at $E_4 = 10$ MeV in ^{18}O was found to have little effect. Neglecting the tail of the nuclear potential was likewise found to have little effect, as shown in Fig. 10.

The energy shift utilized leads to $E_1(2)$ being overpredicted by 12 keV and $E_3(2)$ being overpredicted by 418 keV, compared to the experimental values. Differences of up to a few hundred keV are expected, because the actual Coulomb energy shift includes contributions that depend upon the specific internal structure of the state [77,86]. The constant energy shift was varied to match the energies of the 2_1^+ and 2_3^+ states, and the predicted ANCs and widths were found to not change significantly. Calculations were also performed using level-dependent shifts in Eq. (95a) that allowed all of the $E_i(2)$ to match experiment values. Again, no significant changes in the predicted ANCs or widths were found. In this case, the results become slightly B_c dependent, as discussed in Appendix B. These calculations were done using various B_c values, including values matching the shift function for other levels and $B_c = 0$. None made a significant difference in the predictions.

The dependence of the calculation on the channel radius and the tail of the nuclear potential is shown in Fig. 10, along with calculations treating the levels separately. All calculations converge to the same result for large channel radii, as expected since more of the wave functions are inside the channel radii. Mathematically, the volume renormalization factors approach unity and the shift factors approach zero in this limit. However, the most physically correct channel radius is one just outside the nuclear surface, as discussed in Sec. IV B.

There are some indications that this calculation overpredicts the mixing effects. The width of the 2_3^+ state is overcorrected, with the predicted value of 34.2 keV being about 30% *below* the experimental value. Also, the energy of this state is overpredicted by 421 keV, which is more than expected from differences in the internal Coulomb energy. These issues could be due to channel nonorthogonality, as mentioned in Sec. IV B, since this case has three channels with significant spectroscopic strength. If the channel radius is modestly increased to 4.2 fm, these discrepancies with experiment are much reduced, with the overpredictions of $E_1(2)$ and $E_3(2)$ becoming 28 and 169 keV, respectively, and the prediction for the width of the 2_3^+ state becoming 42.9 keV. The predictions for the $\ell = 0$ C_p^2 for the 2_1^+ and 2_2^+ states are then 16.81 and 159.7 fm^{-1}, respectively. The predictions for channel radii of 3.86 and 4.2 fm are indicated in Fig. 10.

This model of external mixing correctly predicts the striking reduction by a factor of 2–3 in the predicted width of the

2_3^+ state in ^{18}Ne compared to using naive mirror symmetry. Take the average of the $a = 3.86$ and 4.2 fm results, I recommend

$$C_p^2(2_1^+) = 17.4 \pm 2.6 \text{ fm}^{-1} \quad \text{and}$$

$$C_p^2(2_2^+) = 166 \pm 25 \text{ fm}^{-1}, \tag{96}$$

for the $\ell = 0$ ANCs of the first two 2^+ states of ^{18}Ne, using mirror symmetry. The 15% uncertainty is estimated from the various model uncertainties discussed above; the experimental errors on the input mirror ANCs given in Table II contribute an additional 15% uncertainty. The value for the 2_2^+ state is 42% higher than the result of Al-Abdullah *et al.* [75], that was extracted using naive mirror symmetry. This result is 12% higher than the determination of Kuvin *et al.* [76] that does not rely upon mirror symmetry, but this difference is well within their 35% uncertainty. The present result would lead to a somewhat higher reaction rate for ^{17}F$(p, \gamma)^{18}$Ne in novae. A re-evaluation of this rate will not be attempted here. At this time, one is placed in the difficult position of choosing between using the more accurate information available from the mirror nucleus or the less accurate measurements in ^{18}Ne. An improved experimental determination of the 2^+ ANCs in ^{18}Ne would be most helpful here.

The importance of external mixing has been noted previously in this case [73,74,87]. Timofeyuk and Thompson [87] performed three-body calculations considering either two neutrons or two protons outside an inert ^{16}O core. They report smaller mirror symmetry breaking effects than reported here. However, it is known that four-particle–two-hole excitations (i.e., excitations of the ^{16}O core) must be taken into account in order to describe the first three 2^+ states [80], making this difference unsurprising. Calculations using the shell model embedded in the continuum have been reported by Okołowicz *et al.* [74]. For the 2_1^+ state they find an increase in the ratio of the ^{18}Ne to ^{18}O ANCs that is similar to this work. For the 2_2^+ state, they report a decrease in this ratio, in the *opposite* direction of the significant increase found here. They did not report results for the 2_3^+ state. It appears that much of this difference can be attributed to the present calculation being tuned to experimental ANCs in ^{18}O. For example, they report [74, Table VII] squared $\ell = 0$ ANCs for the 2_2^+ state of ^{18}O that are 50–85% larger than the experimental value. If their ^{18}O ANCs for the first two states are used in the present calculations, the discrepancy largely goes away. However, their results for the 2_3^+ state would need be included in order to make a definitive comparison of the two approaches.

C. Discussion

If the off-diagonal components of the matrices in Eqs. (B1), (B2), and (B4) are zero, the transformation process becomes identical to treating the levels independently. This situation would occur if the shift factors were independent of energy and the boundary condition constants were taken equal to these shift factors. It can thus be said that external mixing is driven by the energy dependence of the outgoing-wave boundary condition. However, from this discussion in Sec. II,

this energy dependence is intimately related to the extension of wave functions beyond the channel radius. This quantity is largest near separation thresholds and for low orbital angular momentum. Note also that the energy dependence of the shift factor also gives rise to the volume renormalization factor. The magnitude of the off-diagonal elements is also proportional to the reduced-width amplitudes. The symmetry breaking for the resonant states then results because the ingredients listed above are modified for mirror states by the different charges and separation energies. The 2_2^+ and 2_3^+ states of ^{18}O and ^{18}Ne are thus ideal for exposing this phenomenon since they couple with significant spectroscopic strength to nucleons with $\ell = 0$ and are located near the nucleon separation threshold.

VIII. CONCLUSIONS

This work reviewed the relationship between spectroscopic factors and single-particle wave functions and their physical counterparts, ANCs and widths. R-matrix theory was used extensively to describe these relationships. Also, particular attention was paid to effects arising from beyond the channel radii, which may be termed coupling to the continuum. These effects may be large for levels near a channel threshold, if the level couples significantly to that channel.

A natural application of these concepts is isospin and mirror symmetry. R-matrix theory is an efficient tool to study the symmetry breaking in analog or mirror states arising from differences in the wave functions beyond the channel radii. The examples of single levels in nucleon $+$ ^{12}C, nucleon $+$ ^{16}O, and nucleon $+$ ^{26}Al were studied. It is straightforward to extend this analysis to a group of levels, in which case the continuum coupling may cause a mixing of the levels. The first three 2^+ states of ^{18}O and ^{18}Ne were studied in this manner. It was found that the ANC of the second 2^+ state in ^{18}Ne deduced from the mirror state in ^{18}O is significantly larger than found in previous work. This finding has the effect of increasing the ^{17}F(p, γ)^{18}Ne reaction rate in novae.

The concepts described in this paper arise frequently in the analysis of transfer reaction experiments, the use of theoretical spectroscopic factors to determine ANCs or widths, and the prediction of ANCs or widths using mirror symmetry. It is hoped that this paper will allow future analyses of this type to be carried out with greater confidence and clarity.

ACKNOWLEDGMENTS

APPENDIX A: ALGORITHM FOR COMPUTING $\partial L / \partial E$

The quantity $\partial L / \partial E$, where the derivative is taken with fixed radius and L is the logarithmic radial derivative of the outgoing Coulomb wave defined by Eq. (6), is important for normalizing bound and/or Gamow states, as well as relating observed and reduced widths in R-matrix calculations. Existing methods for calculating this quantity include the numerical differentiation of L values calculated using standard Coulomb function routines and numerical quadrature [88]. For the uncharged case, an analytic result is available; see Gyarmati and Vertse [6, Eq. (6)] and Eqs. (A4) and (A5) below. Here, I present a more efficient and more accurate approach to computing $\partial L / \partial E$ for the general Coulomb case that can be performed in parallel with the calculation of L itself.

Modern numerical routines for the computation of Coulomb wave functions [89–91] use a continued fraction technique to calculate L as an intermediate step for much of the ℓ-ρ-η parameter space. The continued-fraction algorithm is described in detail by Barnett *et al.* [92], and I will utilize their notation and work in terms of the dimensionless variables ρ and η. The approach is to apply the energy derivative to the continued fraction analytically. The derivative ∂E is to be evaluated at fixed radius, implying $\rho \eta$ is constant. Using $\partial \rho / \partial E = \rho / 2E$, one finds

$$\frac{\partial}{\partial E} = \frac{\rho}{2E} \left(\frac{\partial}{\partial \rho} - \frac{\eta}{\rho} \frac{\partial}{\partial \eta} \right), \qquad (A1)$$

when ρ and η are considered independent variables. The outgoing Coulomb wave O satisfies

$$O'' + \left[1 - \frac{2\eta}{\rho} - \frac{\ell(\ell+1)}{\rho^2} \right] O = 0, \qquad (A2)$$

where $' \equiv d/d\rho$. Since $L = \rho O'/O$, one has

$$L' = \frac{O'}{O} + \rho \left[\frac{O''}{O} - \left(\frac{O'}{O} \right)^2 \right] \qquad (A3)$$

and hence

$$L' = \frac{1}{\rho} [L(1 - L) + \ell(\ell+1)] + 2\eta - \rho. \qquad (A4)$$

Defining $\dot{} \equiv \partial / \partial \eta$, one then has

$$\frac{\partial L}{\partial E} = \frac{\rho}{2E} \left(L' - \frac{\eta}{\rho} \dot{L} \right). \qquad (A5)$$

Note that when $\eta = 0$ this equation provides an analytic result that can be expressed in terms of spherical Hankel functions. If $\eta = 0$ and ℓ is an integer, then L and L' are rational functions of ρ and the infinite sequence for L given below terminates.

Steed's algorithm [92, Eq. (32)] provides a sequence of Δh_n and h_n values with

$$h_n = \begin{cases} i(\rho - \eta) & n = 0 \\ h_0 + \sum_{k=1}^{n} \Delta h_k & n > 0 \end{cases} \qquad (A6)$$

such that $\lim_{n \to \infty} h_n = L$. The starting values and recurrence formulas for the Δh_n sequence are given in the first column of

TABLE V. Starting values ($n = 1$) and recurrence formulas ($n > 1$) for the sequences to evaluate L and $\dot{L}$.

L	$\dot{L}$
Starting values	
$a_1 = -\eta^2 - \ell(\ell + 1) + i\eta$	$\dot{a}_1 = -2\eta + i$
$b_1 = 2(\rho - \eta + i)$	$\dot{b}_1 = -2$
$D_1 = 1/b_1$	$\dot{D}_1 = -\dot{b}_1/b_1^2 = 2/b_1^2$
$\Delta h_1 = i a_1 D_1$	$\Delta \dot{h}_1 = i(\dot{a}_1 D_1 + a_1 \dot{D}_1)$
$h_1 = i(\rho - \eta) + \Delta h_1$	$\dot{h}_1 = -i + \Delta \dot{h}_1$
Recurrence formulas	
$a_n = a_{n-1} + 2(n-1) + 2i\eta$	$\dot{a}_n = \dot{a}_{n-1} + 2i$
$b_n = b_{n-1} + 2i$	$\dot{b}_n = \dot{b}_{n-1} = \dot{b}_1 = -2$
$D_n = (D_{n-1}a_n + b_n)^{-1}$	$\dot{D}_n = -\dfrac{\dot{D}_{n-1}a_n + D_{n-1}\dot{a}_n + \dot{b}_n}{(D_{n-1}a_n + b_n)^2}$
$\Delta h_n = (b_n D_n - 1)\Delta h_{n-1}$	$\Delta \dot{h}_n = (\dot{b}_n D_n + b_n \dot{D}_n)\Delta h_{n-1} + (b_n D_n - 1)\Delta \dot{h}_{n-1}$
$h_n = h_{n-1} + \Delta h_n$	$\dot{h}_n = \dot{h}_{n-1} + \Delta \dot{h}_n$

Table V. Differentiating Eq. (A6) with respect to η yields

$$\dot{h}_n = \begin{cases} -i & n = 0 \\ \dot{h}_0 + \sum_{k=1}^{n} \Delta \dot{h}_k & n > 0 \end{cases}. \tag{A7}$$

Assuming that the sum can be differentiated term by term in the limit that $n \to \infty$, one then has

$$\dot{L} = \lim_{n \to \infty} \dot{h}_n. \tag{A8}$$

The starting values and recurrence formulas for the $\Delta \dot{h}_n$ sequence are straightforward to calculate by differentiation and are given in the second column of Table V. Note that L and $\dot{L}$ are calculated in parallel, as the $\dot{L}$ sequence depends upon the L sequence. With L and $\dot{L}$ in hand, $\partial L/\partial E$ may be calculated using Eqs. (A4) and (A5).

A rigorous proof of Eq. (A8) requires showing that the limit of the right-hand side of the equation converges uniformly in η to its limit, which I have not attempted. In practice, the sequence converges in a manner very similar to the h_n sequence. Table VI shows the convergence properties for some of the cases encountered in this work. The quantities $N(L)$ and $N(\dot{L})$ are the n values required to achieve $|\Delta h_n/h_n| < 10^{-13}$ and $|\Delta \dot{h}_n/\dot{h}_n| < 10^{-13}$, respectively. The $\dot{h}_n$ sequence is seen to converge with just a modest number of additional iterations compared to the h_n sequence in every case.

APPENDIX B: *R*-MATRIX PARAMETER TRANSFORMATIONS

Methods for transforming between *R*-matrix eigenfunctions satisfying resonance boundary conditions for all energy levels and a basis satisfying energy-independent boundary conditions have been given by Brune [93]. The N eigenfunctions satisfying resonance boundary conditions correspond to level energy and reduced width parameters E_i and γ_{ic}, where i is the level index and c is the channel index. The parameters corresponding to energy-independent boundary conditions, the assumption of traditional *R*-matrix theory [3,72], are indicated by $\hat{E}_\lambda$ and $\hat{\gamma}_{\lambda c}$. In addition, the boundary condition parameters B_c are assumed to be real and independent of energy and isospin. Note that the present notation differs from that of Ref. [93].

I first consider the transformation $\{E_i, \gamma_{ic}\} \to \{\hat{E}_\lambda, \hat{\gamma}_{\lambda c}, B_c\}$. The matrices M and N are defined with elements given by

$$M_{ij} = \begin{cases} 1 & i = j \\ -\sum_c \gamma_{ic}\gamma_{jc}\dfrac{\hat{S}_{ic} - \hat{S}_{jc}}{E_i - E_j} & i \neq j \end{cases} \tag{B1}$$

and

$$N_{ij} = \begin{cases} E_i + \sum_c \gamma_{ic}^2(\hat{S}_{ic} - B_c) & i = j \\ \sum_c \gamma_{ic}\gamma_{jc}\left(\dfrac{E_i\hat{S}_{jc} - E_j\hat{S}_{ic}}{E_i - E_j} - B_c\right) & i \neq j \end{cases}, \tag{B2}$$

TABLE VI. The number of iterations required to reach a specified convergence (see text) are given by $N(L)$ and $N(\dot{L})$ for L and $\dot{L}$, respectively, for some applications and corresponding values of ℓ, ρ, and η.

ℓ	ρ	η	$N(L)$	$N(\dot{L})$	Application
0	$0.480 - i0.011$	$1.404 + i0.031$	147	157	$420.5 - i18.75$ keV $p + {}^{12}$C, $r = 3.51$ fm
0	$2.735 - i0.061$	$1.404 + i0.031$	35	37	$420.5 - i18.75$ keV $p + {}^{12}$C, $r = 20$ fm
0	$i0.267$	$-i4.261$	136	150	-105.2 keV $p + {}^{17}$F, $r = 3.86$ fm
0	$i1.384$	$-i4.261$	39	44	-105.2 keV $p + {}^{17}$F, $r = 20$ fm
0	0.334	5.662	238	265	126.8 keV $p + {}^{26}$Al, $r = 4.35$ fm
0	1.534	5.662	81	90	126.8 keV $p + {}^{26}$Al, $r = 20$ fm

where the notation $\hat{S}_{ic}$ indicates the shift function evaluated at E_i. Next one solves the real symmetric generalized linear eigenvalue equation

$$(\boldsymbol{N} - \hat{E}_\lambda \boldsymbol{M})\boldsymbol{b}_\lambda = 0. \tag{B3}$$

As discussed in Ref. [93], it is expected that $\boldsymbol{M}$ is positive definite for physically reasonable parameters and the eigenvalue problem can be solved to yield N real eigenvalues and eigenvectors. The eigenvectors $\boldsymbol{b}_\lambda$ may be arranged into a square matrix $\boldsymbol{b}$ and are normalized such that $\boldsymbol{b}^T \boldsymbol{M} \boldsymbol{b} = \boldsymbol{1}$, where $\boldsymbol{1}$ is the unit matrix. The matrix $\boldsymbol{N}$ is also diagonalized by $\boldsymbol{b}$, with $\boldsymbol{b}^T \boldsymbol{N} \boldsymbol{b} = \boldsymbol{e}$, where $e_{\lambda\mu} = \hat{E}_\lambda \delta_{\lambda\mu}$. The reduced widths γ_{ic} and $\hat{\gamma}_{\lambda c}$ may be arranged into column matrices $\boldsymbol{\gamma}_c$ and $\hat{\boldsymbol{\gamma}}_c$ that allow the transformed reduced widths to be written as $\hat{\boldsymbol{\gamma}}_c = \boldsymbol{b}^T \boldsymbol{\gamma}_c$. This completes the transformation to the $\{\hat{E}_\lambda, \hat{\gamma}_{\lambda c}, B_c\}$ basis.

The transformation in the other direction, $\{\hat{E}_\lambda, \hat{\gamma}_{\lambda c}, B_c\} \to \{E_i, \gamma_{ic}\}$, is accomplished by solving the real symmetric nonlinear eigenvalue equation

$$\left\{ \boldsymbol{e} - E_i \boldsymbol{1} - \sum_c \hat{\boldsymbol{\gamma}}_c [\hat{S}_c(E_i) - B_c] \hat{\boldsymbol{\gamma}}_c^T \right\} \boldsymbol{a}_i = 0 \tag{B4}$$

for eigenvalues E_i and eigenvectors $\boldsymbol{a}_i$. As discussed in Ref. [93], this equation has N real eigenvalues if $\partial \hat{S}_c / \partial E \geqslant 0$. This condition is always met when the potential outside the channel radius consists of the repulsive Coulomb and angular momentum barriers [94]. The tail of the attractive nuclear potential included in the calculations presented here could spoil this situation, but in this work the derivative has been found to be positive, for the potential strengths and energy ranges considered. This question would need to be revisited for $\ell = 0$ neutron channels with positive energy, where there is no Coulomb or angular momentum barrier and any attractive potential will likely create a negative energy derivative. The solution of nonlinear eigenvalue problems has been reviewed by Voss [95]. If the energy derivative of the shift function is positive, the eigenvalue problem is characterized as overdamped, which provides several nice mathematical properties [95,96], including the existence of N real eigenvalues noted above. For this work, I have solved the eigenvalue equation using the *safeguarded iteration* algorithm [95]. The eigenvectors are normalized such that $\boldsymbol{a}_i^T \boldsymbol{a}_i = 1$ and $\gamma_{ic} = \boldsymbol{a}_i^T \hat{\boldsymbol{\gamma}}_c$, completing the transformation.

The mirror transformation $\{E_i(1), \gamma_{ic}(1)\} \to \{E_i(2), \gamma_{ic}(2)\}$ is implemented as follows, where (1) and (2) indicate the initial and final nuclei. First, the resonance parameters $\{E_i(1), \gamma_{ic}(1)\}$ are transformed to $\{\hat{E}_\lambda(1), \hat{\gamma}_{\lambda c}(1), B_c\}$. In this basis, the boundary conditions satisfied by the eigenfunctions

are independent of isospin. The transformation is then applied using Eq. (95). Finally, one transforms $\{\hat{E}_\lambda(2), \hat{\gamma}_{\lambda c}(2), B_c\} \to \{E_i(2), \gamma_{ic}(2)\}$.

When not considering mirror symmetry, $\{E_i, \gamma_{ic}\}$ and physical observables are independent of the B_c, even when the number of levels in finite [93,97,98]. The question of B_c invariance under the mirror transformation is investigated as follows. Equation (B4) becomes

$$\left\{ \boldsymbol{e}(1) + \boldsymbol{\Delta} - E_i(2)\boldsymbol{1} \right. $$
$$\left. - \sum_c \hat{\boldsymbol{\gamma}}_c(1)[\hat{S}_c(E_i(2)) - B_c] \hat{\boldsymbol{\gamma}}_c^T(1) \right\} \boldsymbol{a}_i = 0, \tag{B5}$$

where the components of $\boldsymbol{\Delta}$ are given by $\Delta_\lambda \delta_{\lambda\mu}$. Note also that the charge used to evaluate the shift function must also change when $1 \to 2$. The transformation to different boundary conditions, $\{\hat{E}_\lambda(1), \hat{\gamma}_{\lambda c}(1), B_c\} \to \{\hat{E}'_\lambda(1), \hat{\gamma}'_{\lambda c}(1), B'_c\}$, is given by [98]

$$\boldsymbol{e}'(1) = \boldsymbol{K}\boldsymbol{C}\boldsymbol{K}^T \quad \text{and} \quad \hat{\boldsymbol{\gamma}}'_c(1) = \boldsymbol{K}\hat{\boldsymbol{\gamma}}_c(1), \tag{B6}$$

where the real orthogonal matrix $\boldsymbol{K}$ diagonalizes

$$\boldsymbol{C} = \boldsymbol{e}(1) - \sum_c \hat{\boldsymbol{\gamma}}_c(1)(B'_c - B_c)\hat{\boldsymbol{\gamma}}_c^T(1). \tag{B7}$$

With $\boldsymbol{a}'_i = \boldsymbol{K}\boldsymbol{a}_i$, Eq. (B5) becomes

$$\left\{ \boldsymbol{e}'(1) + \boldsymbol{K}\boldsymbol{\Delta}\boldsymbol{K}^T - E_i(2)\boldsymbol{1} \right. $$
$$\left. - \sum_c \hat{\boldsymbol{\gamma}}'_c(1)[\hat{S}_c(E_i(2)) - B'_c] \hat{\boldsymbol{\gamma}}'^T_c(1) \right\} \boldsymbol{a}'_i = 0. \tag{B8}$$

If $[\boldsymbol{K}, \boldsymbol{\Delta}] = 0$, then this equation becomes

$$\left\{ \boldsymbol{e}'(1) + \boldsymbol{\Delta} - E_i(2)\boldsymbol{1} \right. $$
$$\left. - \sum_c \hat{\boldsymbol{\gamma}}'_c(1)[\hat{S}_c(E_i(2)) - B'_c] \hat{\boldsymbol{\gamma}}'^T_c(1) \right\} \boldsymbol{a}'_i = 0, \tag{B9}$$

which is of the same form as Eq. (B5) and has the same energy shifts. The two equations are related by the similarity transformation $\boldsymbol{K}$. In this case, the eigenvalues $E_i(2)$ and reduced widths $\gamma_{ic}(2) = \boldsymbol{a}_i^T \hat{\boldsymbol{\gamma}}_c(2) = \boldsymbol{a}_i'^T \hat{\boldsymbol{\gamma}}'_c(2)$ are invariant under change of boundary condition. However, the more general procedure is somewhat B_c dependent.

For the case of a constant Coulomb energy shift applied to all levels, $\boldsymbol{\Delta} = \Delta\boldsymbol{1}$, the commutator $[\boldsymbol{K}, \boldsymbol{\Delta}] = 0$. Thus, in this particular situation, the procedure is exactly B_c independent. In the limit of a large number of levels, the various bases are complete and the more general procedure would also be expected to become B_c independent.

[1] D. W. Bardayan, Transfer reactions in nuclear astrophysics, J. Phys. G: Nucl. Part. Phys. **43**, 043001 (2016).

[2] C. R. Brune and B. Davids, Radiative capture reactions in astrophysics, Annu. Rev. Nucl. Part. Sci. **65**, 87 (2015).

[3] A. M. Lane and R. G. Thomas, *R*-matrix theory of nuclear reactions, Rev. Mod. Phys. **30**, 257 (1958).

[4] A. Messiah, *Quantum Mechanics* (North-Holland, Amsterdam, 1961), Vol. 1.

[5] Y. B. Zel'dovich, On the theory of unstable states, Sov. Phys. JETP **12**, 542 (1961).

[6] B. Gyarmati and T. Vertse, On the normalization of Gamow functions, Nucl. Phys. A **160**, 523 (1971).

[7] G. García-Calderón and R. Peierls, Resonant states and their uses, Nucl. Phys. A **265**, 443 (1976).

[8] J. Humblet and L. Rosenfeld, Theory of nuclear reactions: I. Resonant states and collision matrix, Nucl. Phys. **26**, 529 (1961).

[9] A. T. Kruppa and W. Nazarewicz, Gamow and R-matrix approach to proton emitting nuclei, Phys. Rev. C **69**, 054311 (2004).

[10] J. Humblet, K-matrix analysis of resonance nuclear reactions, Phys. Rev. C **42**, 1582 (1990).

[11] H. O. Meyer, G. R. Plattner, and I. Sick, Elastic $p + {}^{12}$C scattering between 0.3 and 2 MeV, Z. Phys. A **279**, 41 (1976).

[12] S. Daigle, K. J. Kelly, A. E. Champagne, M. Q. Buckner, C. Iliadis, and C. Howard, Measurement of the $E_r^{\mathrm{c.m.}} = 259$ keV resonance in the ^{14}N$(p, \gamma){}^{15}$O reaction, Phys. Rev. C **94**, 025803 (2016).

[13] G. Lotay, P. J. Woods, D. Seweryniak, M. P. Carpenter, H. M. David, R. V. F. Janssens, and S. Zhu, Identification of analog states in the $T = 1/2$ $A = 27$ mirror system from low excitation energies to the region of hydrogen burning in the ^{26}Al$^{g,m}(p, \gamma){}^{27}$Si reactions, Phys. Rev. C **84**, 035802 (2011).

[14] M. Wang, G. Audi, F. G. Kondev, W. J. Huang, S. Naimi, and X. Xu, The AME2016 atomic mass evaluation (II): Tables, graphs, and references, Chin. Phys. C **41**, 030003 (2017).

[15] H. T. Fortune, Definitions of a single-particle resonance, Phys. Rev. C **73**, 014318 (2006).

[16] P. D. Kunz, DWUCK-CHUCK: Nuclear model code system for distorted wave Born approximation and coupled channel calculations, Radiation Safety Information Computational Center, PSR-546 (Oak Ridge National Laboratory, Oak Ridge, Tennessee, 2008).

[17] A. M. Lane and D. Robson, Comprehensive formalism for nuclear reaction problems. I. Derivation of existing reaction theories, Phys. Rev. **151**, 774 (1966).

[18] P. L. Kapur and R. Peierls, The dispersion formula for nuclear reactions, Proc. R. Soc. London A **166**, 277 (1938).

[19] C. Iliadis, Proton single-particle reduced widths for unbound states, Nucl. Phys. A **618**, 166 (1997).

[20] C. H. Johnson, Unified R-matrix-plus-potential analysis for ^{16}O$+n$ cross sections, Phys. Rev. C **7**, 561 (1973).

[21] A. M. Lane, A theory of anomalies observed in (d, p) excitation curves at thresholds for neutron analogue channels, Phys. Lett. B **33**, 274 (1970).

[22] A. M. Lane and P. E. Hodgson, Behaviour of single-particle states and their eigenvalues near zero energy, Ann. Phys. **106**, 44 (1977).

[23] F. C. Barker, A model for nuclear threshold levels, Proc. Phys. Soc. **84**, 681 (1964).

[24] T. Berggren, Overlap integrals and single-particle wave functions in direct interaction theories, Nucl. Phys. **72**, 337 (1965).

[25] W. T. Pinkston and G. R. Satchler, Form factors for nuclear stripping reactions, Nucl. Phys. **72**, 641 (1965).

[26] N. K. Timofeyuk, R. C. Johnson, and A. M. Mukhamedzhanov, Relation between Proton and Neutron Asymptotic Normalization Coefficients for Light Mirror Nuclei and its Relevance to Nuclear Astrophysics, Phys. Rev. Lett. **91**, 232501 (2003).

[27] N. Michel, W. Nazarewicz, M. Płoszajczak, and T. Vertse, Shell model in the complex energy plane, J. Phys. G: Nucl. Part. Phys. **36**, 013101 (2008).

[28] N. K. Timofeyuk, Overlap functions, spectroscopic factors, and asymptotic normalization coefficients generated by a shell-model source term, Phys. Rev. C **81**, 064306 (2010).

[29] K. M. Nollett and R. B. Wiringa, Asymptotic normalization coefficients from *ab initio* calculations, Phys. Rev. C **83**, 041001(R) (2011).

[30] N. K. Timofeyuk, Properties of one-nucleon overlap functions for $A \geqslant 16$ double-closed-shell nuclei in the source-term approach, Phys. Rev. C **84**, 054313 (2011).

[31] K. M. Nollett, *Ab initio* calculations of nuclear widths via an integral relation, Phys. Rev. C **86**, 044330 (2012).

[32] A. M. Mukhamedzhanov, Connection between asymptotic normalization coefficients and resonance widths of mirror states, Phys. Rev. C **99**, 024311 (2019).

[33] I. J. Thompson and F. M. Nunes, *Nuclear Reactions for Astrophysics: Principles, Calculation, and Applications of Low-Energy Reactions* (Cambridge University Press, Cambridge, UK, 2009).

[34] J. L. Friar, Measurability of the deuteron D state probability, Phys. Rev. C **20**, 325 (1979).

[35] A. M. Mukhamedzhanov and A. S. Kadyrov, Unitary correlation in nuclear reaction theory: Separation of nuclear reactions and spectroscopic factors, Phys. Rev. C **82**, 051601(R) (2010).

[36] W. J. Thompson, J. L. Adams, and D. Robson, Neutron spectroscopic factors from isobaric analog states, Phys. Rev. **173**, 975 (1968).

[37] D. Robson, Theory of nucleon induced analogue resonances, in *Isospin in Nuclear Physics*, edited by D. H. Wilkinson (North-Holland, Amsterdam, 1969), pp. 461–508.

[38] G. D. Westin and J. L. Adams, Potential scattering and spectroscopic factors in R-matrix theory, Phys. Rev. C **4**, 363 (1971).

[39] S. E. Koonin, T. A. Tombrello, and G. Fox, A "hybrid" R-matrix-optical model parametrization of the ^{12}C$(\alpha, \gamma){}^{16}$O cross section, Nucl. Phys. A **220**, 221 (1974).

[40] J. B. French, The analysis of reduced widths, in *Nuclear Spectroscopy*, edited by F. Ajzenberg-Selov (Academic Press, New York, 1960), pp. 890–931.

[41] M. H. Macfarlane and J. B. French, Stripping reactions and the structure of light and intermediate nuclei, Rev. Mod. Phys. **32**, 567 (1960).

[42] F. C. Barker, Comment on "Proton single-particle reduced widths for unbound states", Nucl. Phys. A **637**, 576 (1998).

[43] F. C. Barker, Comment on "Spectroscopic factors for bound s-wave states derived from neutron scattering lengths", Phys. Rev. C **56**, 3423 (1997).

[44] P. Mohr, H. Herndl, H. Oberhummer, and G. Staudt, Reply to "Comment on 'Spectroscopic factors for bound s-wave states derived from neutron scattering lengths' ", Phys. Rev. C **56**, 3425 (1997).

[45] P. Descouvemont and D. Baye, The R-matrix theory, Rep. Prog. Phys. **73**, 036301 (2010).

[46] C. Werntz and W. E. Meyerhof, ^{4}He levels from a charge-independent analysis of ^{3}H$(p, n){}^{3}$He, Nucl. Phys. A **121**, 38 (1968).

[47] J. E. Monahan, H. T. Fortune, C. M. Vincent, and R. E. Segel, $T = 1$ states in the $A = 12$ system, Phys. Rev. C **3**, 2192 (1971).

[48] G. M. Hale, D. C. Dodder, J. D. Seagrave, B. L. Berman, and T. W. Phillips, Neutron-triton cross sections and scattering lengths obtained from $p-{}^{3}$He scattering, Phys. Rev. C **42**, 438 (1990).

[49] F. C. Barker and N. Ferdous, The low-lying levels of ^{13}C and ^{13}N, Aust. J. Phys. **33**, 691 (1980).

[50] F. C. Barker, Masses of exotic nuclei and the Thomas-Ehrman shift, in *Structure and Reactions of Unstable Nuclei, Proceedings of the International Symposium, Niigata, Japan, 1991*, edited by K. Ikeda and Y. Suzuki (World Scientific, Singapore, 1992), pp. 33–39.

[51] R. G. Thomas, An analysis of the energy levels of the mirror nuclei, ^{13}C and ^{13}N, Phys. Rev. **88**, 1109 (1952).

[52] J. B. Ehrman, On the displacement of corresponding energy levels of ^{13}C and ^{13}N, Phys. Rev. **81**, 412 (1951).

[53] K. G. Bernhardt, W. R. Hering, P. Ring, and E. Werner, Wave functions of nuclear states with small single-particle spectroscopic factors, Nucl. Phys. A **249**, 329 (1975).

[54] J. S. Winfield, N. A. Jelley, W. D. M. Rae, and C. L. Woods, Spectroscopic-factor discrepancies in (^{9}Be, ^{10}B) for different ejectile excitations, Nucl. Phys. A **437**, 65 (1985).

[55] N. K. Timofeyuk and P. Descouvemont, Asymptotic normalization coefficients for mirror virtual nucleon decays in a microscopic cluster model, Phys. Rev. C **71**, 064305 (2005).

[56] N. K. Timofeyuk and P. Descouvemont, Relation between widths of proton resonances and neutron asymptotic normalization coefficients in mirror states of light nuclei in a microscopic cluster model, Phys. Rev. C **72**, 064324 (2005). Note that the $'$ in Eq. (20) of this paper indicates differentiation with respect energy, while the $'$ in the following equation that defines S_l indicates differentiation with respect to κa.

[57] N. K. Timofeyuk, P. Descouvemont, and R. C. Johnson, Isospin symmetry in mirror α decays, Phys. Rev. C **75**, 034302 (2007).

[58] L. I. Schiff, *Quantum Mechanics*, 3rd ed. (McGraw-Hill, New York, 1968).

[59] Z. H. Liu, C. J. Lin, H. Q. Zhang, Z. C. Li, J. S. Zhang, Y. W. Wu, F. Yang, M. Ruan, J. C. Liu, S. Y. Li, and Z. H. Peng, Asymptotic normalization coefficients and neutron halo of the excited states in ^{12}B and ^{13}C, Phys. Rev. C **64**, 034312 (2001).

[60] N. Imai, N. Aoi, S. Kubono, D. Beaumel, K. Abe, S. Kato, T. Kubo, K. Kumagai, M. Kurokawa, X. Liu, A. Mengoni, S. Michimasa, H. Ohnuma, H. Sakurai, P. Strasser, T. Teranishi, and M. Ishihara, Test of the ANC method via (d, p) reaction, Nucl. Phys. A **688**, 281c (2001).

[61] B. Guo, Z.-H. Li, W.-P. Liu, and X.-X. Bai, Test of determination of (p, γ) astrophysical S-factors using the asymptotic normalization coefficients from neutron transfer reactions, Chin. Phys. Lett. **24**, 2544 (2007).

[62] S. V. Artemov, É. A. Zaparov, M. A. Kayumov, and G. K. Nie, Proton-separation vertex constants for sd-shell nuclei from an analysis of peripheral transfer reactions, Phys. At. Nucl. **63**, 1763 (2000).

[63] C. A. Gagliardi, R. E. Tribble, A. Azhari, H. L. Clark, Y.-W. Lui, A. M. Mukhamedzhanov, A. Sattarov, L. Trache, V. Burjan, J. Cejpek, V. Kroha, Š. Piskoř, and J. Vincour, Tests of transfer reaction determinations of astrophysical S factors, Phys. Rev. C **59**, 1149 (1999).

[64] C. R. Brune, A comparison of K- and R-matrix parameterizations of s-wave ^{16}O $+p$ elastic scattering, Nucl. Phys. A **596**, 122 (1996).

[65] C. Iliadis, C. Angulo, P. Descouvemont, M. Lugaro, and P. Mohr, New reaction rate for ^{16}O(p, γ) ^{17}F and its influence on the oxygen isotopic ratios in massive AGB stars, Phys. Rev. C **77**, 045802 (2008).

[66] N. K. Timofeyuk, P. Descouvemont, and R. C. Johnson, Relation between proton and neutron asymptotic normalization coefficients for light mirror nuclei and its relevance for nuclear astrophysics, Eur. Phys. J. A **27**, 269 (2006).

[67] L. J. Titus, P. Capel, and F. M. Nunes, Asymptotic normalization of mirror states and the effect of couplings, Phys. Rev. C **84**, 035805 (2011).

[68] S. D. Pain, D. W. Bardayan, J. C. Blackmon, S. M. Brown, K. Y. Chae, K. A. Chipps, J. A. Cizewski, K. L. Jones, R. L. Kozub, J. F. Liang, C. Matei, M. Matos, B. H. Moazen, C. D. Nesaraja, J. Okołowicz, P. D. O'Malley, W. A. Peters, S. T. Pittman, M. Płoszajczak, K. T. Schmitt, J. F. Shriner, D. Shapira, M. S. Smith, D. W. Stracener, and G. L. Wilson, Constraint of the Astrophysical ^{26g}Al(p, γ) ^{27}Si Destruction Rate at Stellar Temperatures, Phys. Rev. Lett. **114**, 212501 (2015).

[69] V. Margerin, G. Lotay, P. J. Woods, M. Aliotta, G. Christian, B. Davids, T. Davinson, D. T. Doherty, J. Fallis, D. Howell, O. S. Kirsebom, D. J. Mountford, A. Rojas, C. Ruiz, and J. A. Tostevin, Inverse Kinematic Study of the ^{26g}Al(d, p) ^{27}Al Reaction and Implications for Destruction of ^{26}Al in Wolf-Rayet and Asymptotic Giant Branch Stars, Phys. Rev. Lett. **115**, 062701 (2015).

[70] V. Margerin, Transfer reaction measurements and the stellar nucleosynthesis of ^{26}Al and ^{44}Ti, Ph.D. thesis, University of Edinburgh, Edinburgh, Scotland, UK, 2016, http://cds.cern.ch/record/2243058.

[71] G. Lotay, P. J. Woods, M. Moukaddam, M. Aliotta, G. Christian, B. Davids, T. Davinson, D. T. Doherty, D. Howell, V. Margerin, and C. Ruiz, High-resolution radioactive beam study of the ^{26}Al(d, p) reaction and measurements of single-particle spectroscopic factors, Eur. Phys. J. A **56**, 3 (2020).

[72] E. P. Wigner and L. Eisenbud, Higher angular momenta and long range interaction in resonance reactions, Phys. Rev. **72**, 29 (1947).

[73] R. Chatterjee, J. Okołowicz, and M. Płoszajczak, Description of the ^{17}F(p, γ) ^{18}Ne radiative capture reaction in the continuum shell model, Nucl. Phys. A **764**, 528 (2006).

[74] J. Okołowicz, N. Michel, W. Nazarewicz, and M. Płoszajczak, Asymptotic normalization coefficients and continuum coupling in mirror nuclei, Phys. Rev. C **85**, 064320 (2012).

[75] T. Al-Abdullah, F. Carstoiu, X. Chen, H. L. Clark, C. A. Gagliardi, Y.-W. Lui, A. Mukhamedzhanov, G. Tabacaru, Y. Tokimoto, L. Trache, R. E. Tribble, and Y. Zhai, Astrophysical reaction rate for ^{17}F(p, γ) ^{18}Ne from the transfer reaction ^{13}C$(^{17}$O, ^{18}O$)$ ^{12}C, Phys. Rev. C **89**, 025809 (2014).

[76] S. A. Kuvin, J. Belarge, L. T. Baby, J. Baker, I. Wiedenhöver, P. Höflich, A. Volya, J. C. Blackmon, C. M. Deibel, H. E. Gardiner, J. Lai, L. E. Linhardt, K. T. Macon, B. C. Rasco, N. Quails, K. Colbert, D. L. Gay, and N. Keeley, Measurement of ^{17}F(d, n) ^{18}Ne and the impact on the ^{17}F(p, γ) ^{18}Ne reaction rate for astrophysics, Phys. Rev. C **96**, 045812 (2017).

[77] A. V. Nero, E. G. Adelberger, and F. S. Dietrich, Structure of ^{18}Ne, Phys. Rev. C **24**, 1864 (1981).

[78] K. I. Hahn, A. García, E. G. Adelberger, P. V. Magnus, A. D. Bacher, N. Bateman, G. P. A. Berg, J. C. Blackmon, A. E. Champagne, B. Davis, A. J. Howard, J. Liu, B. Lund, Z. Q. Mao, D. M. Markoff, P. D. Parker, M. S. Smith, E. J. Stephenson, K. B. Swartz, S. Utku, R. B. Vogelaar, and K. Yildiz, Structure of ^{18}Ne and the breakout from the hot CNO cycle, Phys. Rev. C **54**, 1999 (1996).

[79] T. K. Li, D. Dehnhard, R. E. Brown, and P. J. Ellis, Investigation of the $(d_{5/2})^2$ and $(d_{5/2}s_{1/2})$ two-particle configurations in ^{18}O using the ^{17}O(d, p) ^{18}O reaction at 18 MeV, Phys. Rev. C **13**, 55 (1976).

[80] R. L. Lawson, F. J. D. Serduke, and H. T. Fortune, Structure of low-lying positive-parity states of ^{18}O, Phys. Rev. C **14**, 1245 (1976).

[81] J. Gómez del Campo, A. Galindo-Uribarri, J. R. Beene, C. J. Gross, J. F. Liang, M. L. Halbert, D. W. Stracener, D. Shapira, R. L. Varner, E. Chavez-Lomeli, and M. E. Ortiz, Decay of a Resonance in ^{18}Ne by the Simultaneous Emission of Two Protons, Phys. Rev. Lett. **86**, 43 (2001).

[82] S.-J. Jin, Y.-B. Wang, B.-X. Wang, X.-X. Bai, X. Fang, B. Guo, E.-T. Li, Y.-J. Li, Z.-H. Li, G. Lian, J. Su, S.-Q. Yan, S. Zeng, Z.-E. Yao, and W.-P. Liu, Excited states in ^{18}Ne studied via ^{17}F$+p$, Chin. Phys. Lett. **27**, 032102 (2010).

[83] S. Almaraz-Calderon, W. P. Tan, A. Aprahamian, B. Bucher, A. Roberts, M. Wiescher, C. R. Brune, T. N. Massey, N. Özkan, R. T. Güray, and H. Mach, Level structure of ^{18}Ne and its importance in the ^{14}O(α, p) ^{17}F reaction rate, Phys. Rev. C **86**, 025801 (2012).

[84] B. A. Brown and W. D. M. Rae, The shell-model code NuShellX@MSU, Nucl. Data Sheets **120**, 115 (2014).

[85] A. P. Zuker, B. Buck, and J. B. McGrory, Structure of ^{16}O, Phys. Rev. Lett. **21**, 39 (1968).

[86] R. Sherr and H. T. Fortune, Coulomb energies in ^{18}Ne, Phys. Rev. C **58**, 3292 (1998).

[87] N. K. Timofeyuk and I. J. Thompson, Spectroscopic factors and asymptotic normalization coefficients in mirror three-body systems, Phys. Rev. C **78**, 054322 (2008).

[88] T. Vertse, K. F. Pál, and Z. Balogh, GAMOW, a program for calculating the resonant state solution of the radial Schrödinger equation in an arbitrary optical potential, Comput. Phys. Commun. **27**, 309 (1982).

[89] I. J. Thompson and A. R. Barnett, COULCC: A continued-fraction algorithm for Coulomb functions of complex order with complex arguments, Comput. Phys. Commun. **36**, 363 (1985).

[90] I. J. Thompson and A. R. Barnett, Coulomb and Bessel functions of complex arguments and order, J. Comput. Phys. **64**, 490 (1986).

[91] N. Michel, Precise Coulomb wave functions for a wide range of complex ℓ, η, and z, Comput. Phys. Commun. **176**, 232 (2007).

[92] A. R. Barnett, D. H. Feng, J. W. Steed, and L. J. B. Goldfarb, Coulomb wave functions for all real η and ρ, Comput. Phys. Commun. **8**, 377 (1974).

[93] C. R. Brune, Alternative parametrization of R-matrix theory, Phys. Rev. C **66**, 044611 (2002).

[94] C. R. Brune, G. M. Hale, and M. W. Paris, Monotonic properties of the shift and penetration factors, Phys. Rev. C **97**, 024603 (2018).

[95] H. Voss, Nonlinear eigenvalue problems, in *Handbook of Linear Algebra*, 2nd ed., edited by L. Hogben (CRC Press, Boca Raton, FL, 2014), Chap. 60.

[96] E. H. Rogers, A mimmax theory for overdamped systems, Arch. Ration. Mech. Anal. **16**, 89 (1964).

[97] A. Mori, Boundary-condition constants of the Lane-Robson calculable theory, Phys. Rev. C **5**, 1795 (1972).

[98] F. C. Barker, The boundary condition parameter in R-matrix theory, Aust. J. Phys. **25**, 341 (1972).